(1) Sample	(2) Flux limits	(3) Area of sky	(4) No. of sources	(5) Reference
B2	$1\mathrm{Jy} < \mathrm{S}_{408} < 2\mathrm{Jy}$	$\mathrm{RA} < 13^{\mathrm{h}}02^{\mathrm{m}}; 34^\circ < \delta < 40^\circ; \mathrm{b} > 30^\circ$	59	Allington-Smith
6C	$2.2\mathrm{Jy} < \mathrm{S}_{151} < 4.4\mathrm{Jy}$	$08^{\mathrm{h}}20^{\mathrm{m}} < \mathrm{RA} < 13^{\mathrm{h}}01^{\mathrm{m}}; 34^\circ < \delta < 40^\circ$	68	Eales (1985)

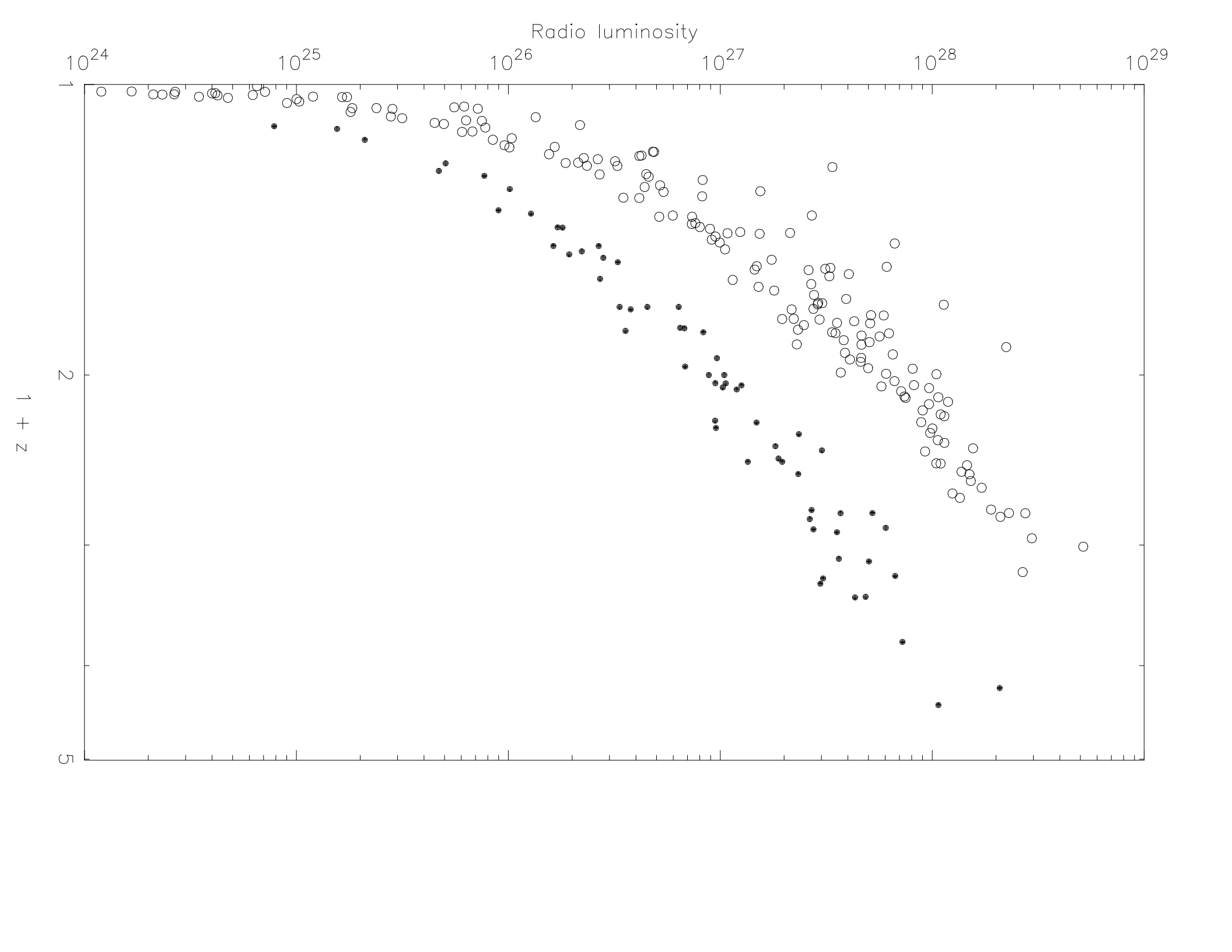
Radio luminosity
10^{24}
10^{25}
10^{26}
10^{27}
10^{28}
10^{29}
1
2
5
1 + z

(1) Name	(2) IRCAM exposure (min)	(3) REDEYE exposure (min)	(4) IRCAM3 exposure (min)
0820+36	21	....	....
0822+34B	27	....	....
0822+39	....	31	....
0825+34	48	....	....
0848+34	27	....	....
0901+35	21	....	....
0905+39	24	35	....
0918+36	27	....	....
0943+39	48	30	27
1011+36	14	45	....
1016+36	69	....	....
1017+37	27	26	....
1042+39	27	....	....
1045+34	42	52	....
1045+35A	21	....	....
1045+35B	21	....	....
1100+35	....	....	18
1123+34	21	45	....
1129+37	....	47	27
1141+35	42	....	....
1143+37	21	....	....
1204+37	63	....	....
1204+35	....	42	27
1212+38	42	....	....
1217+36	....	27	27
1230+34	21	....	....
1256+36	....	42	27
1257+36	21	22	....
1301+35	21	....	....

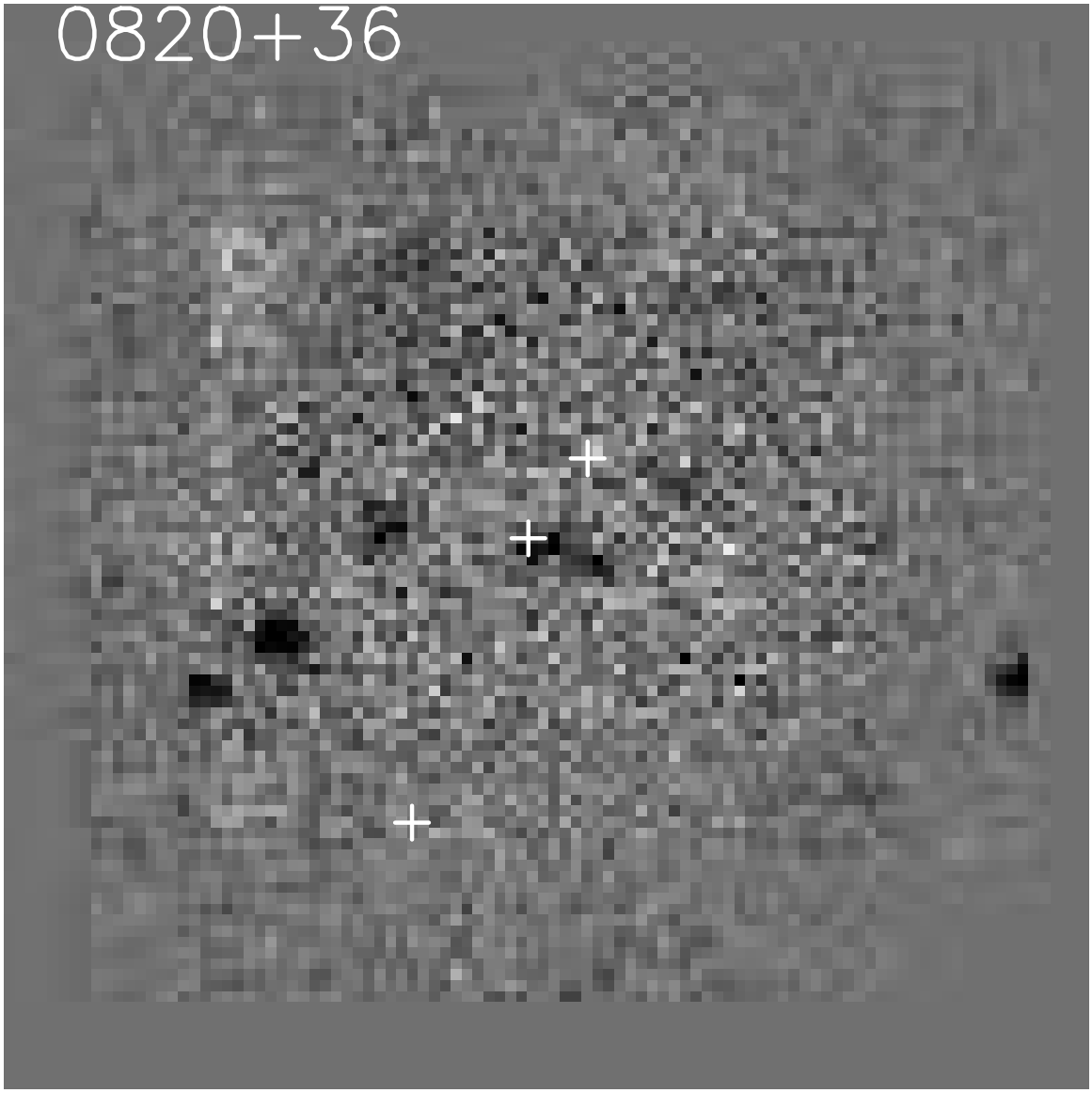
0820+36

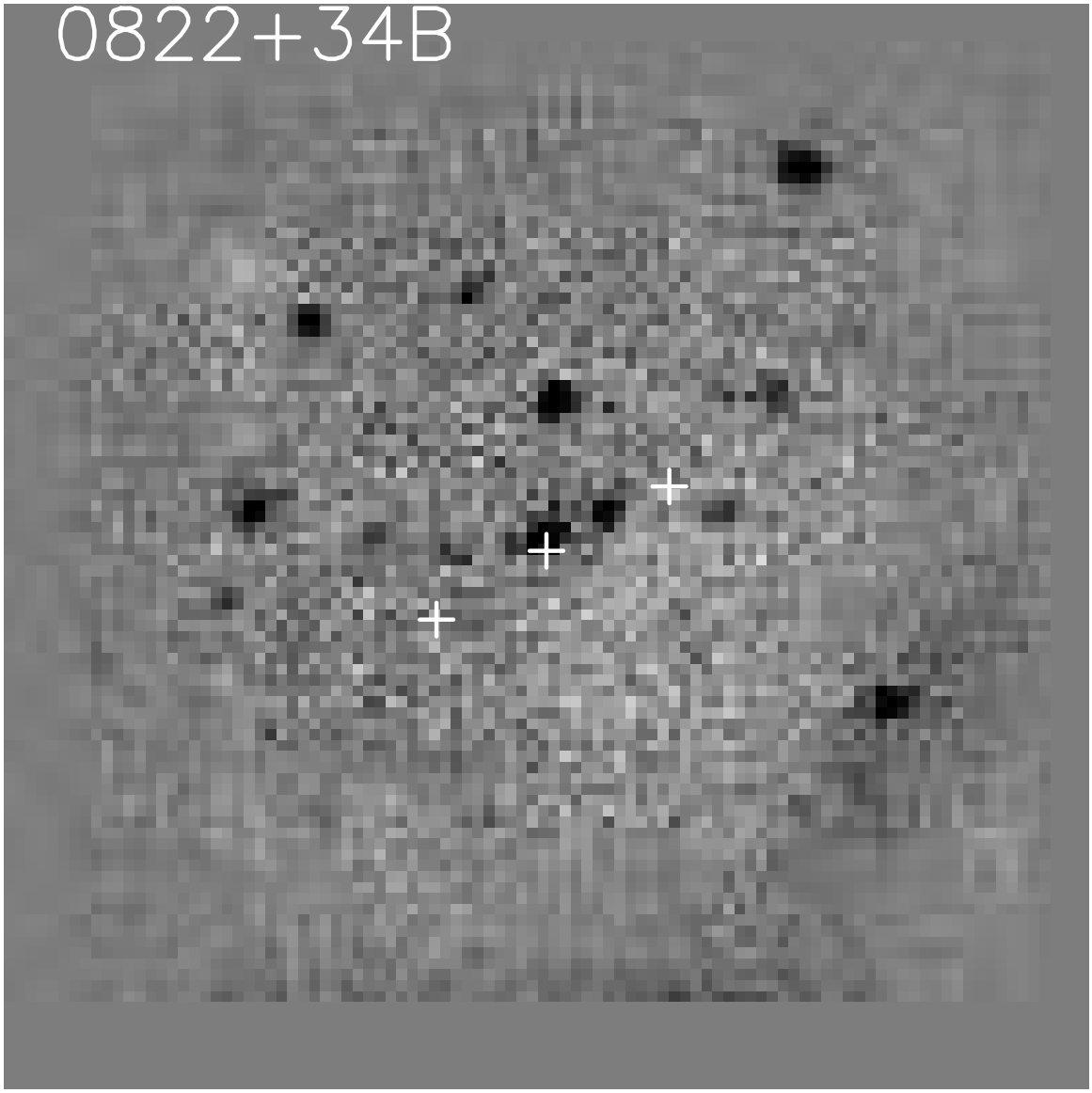
0822+34B

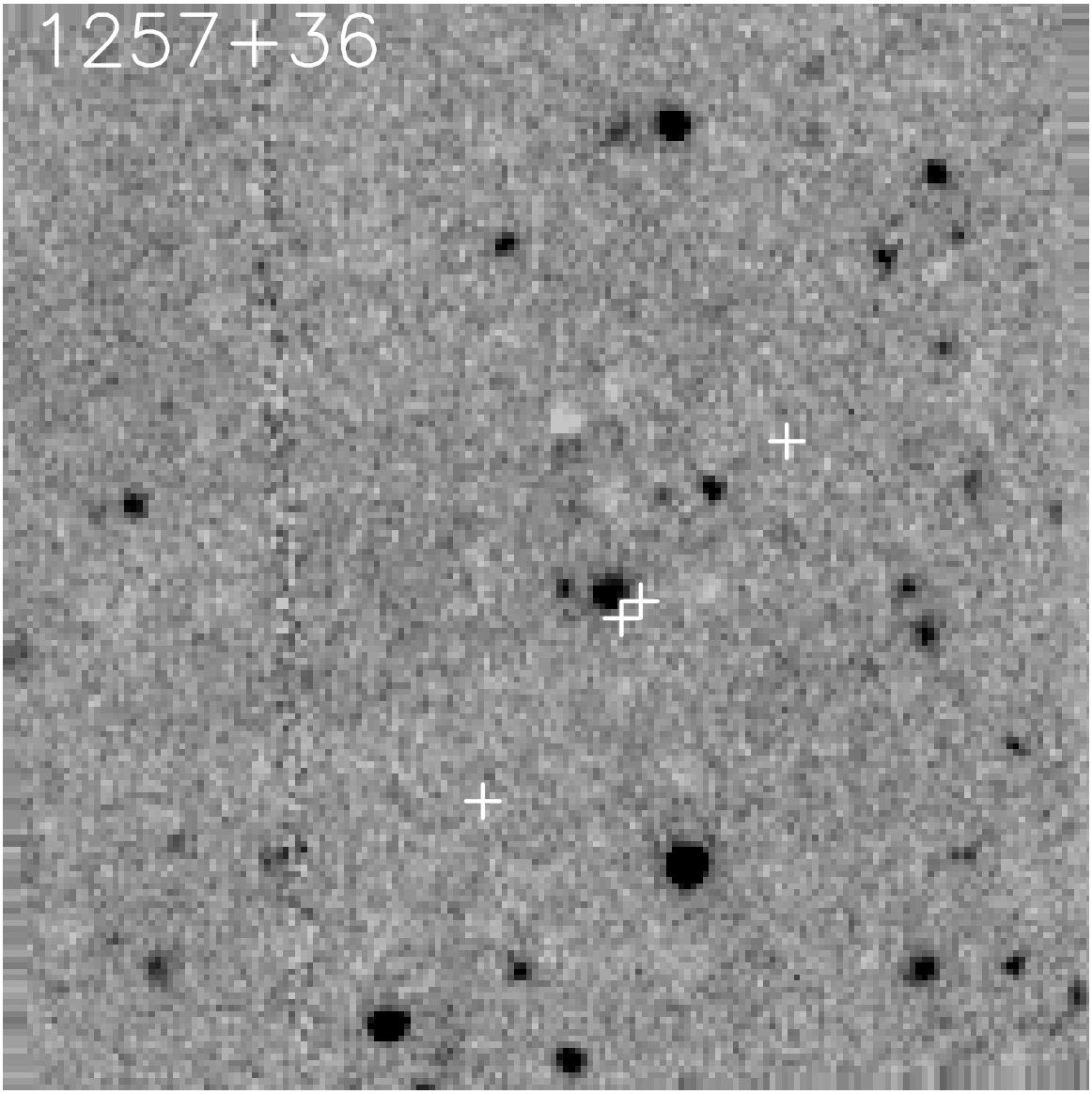
1257+36

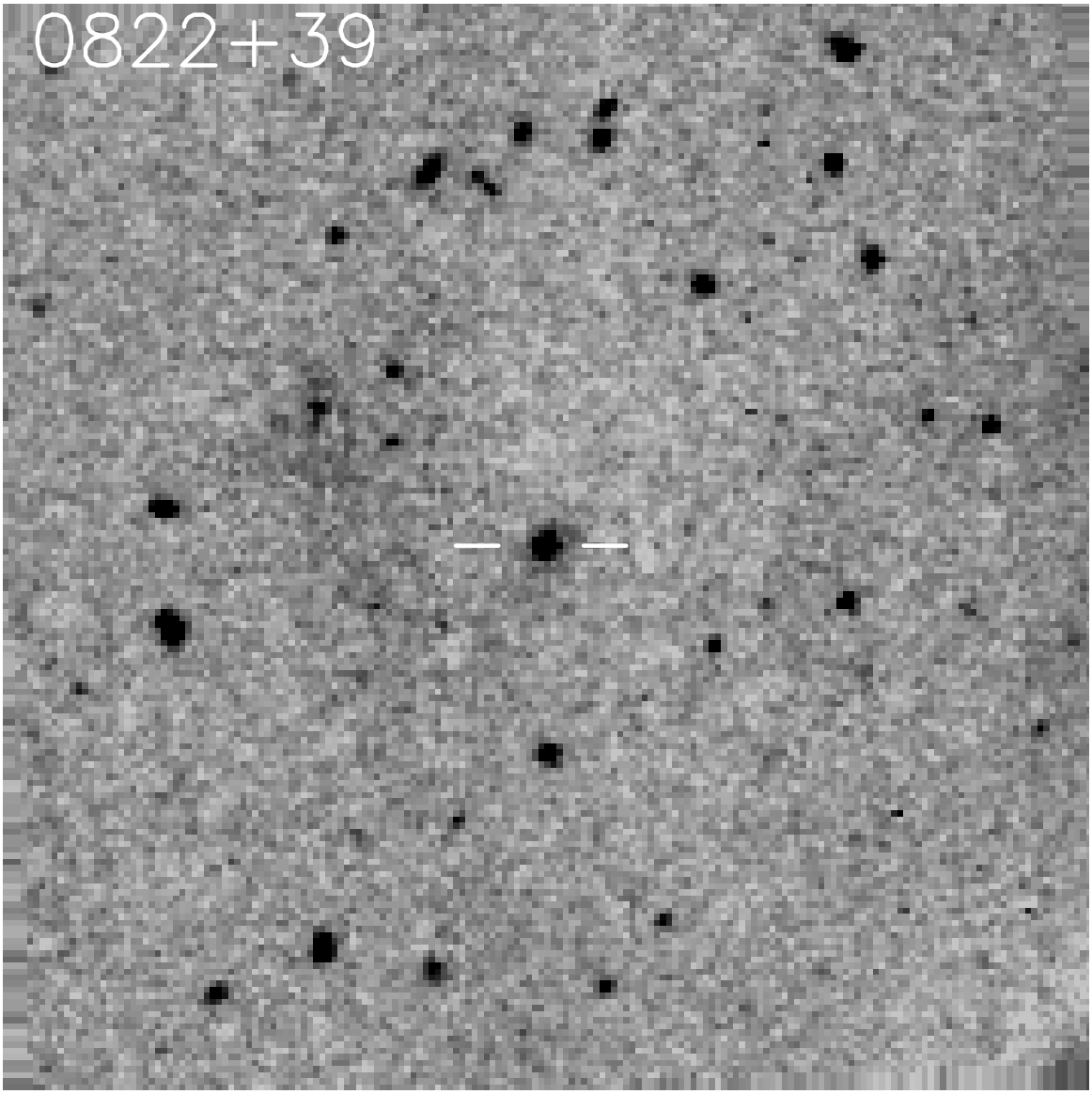
0822+39

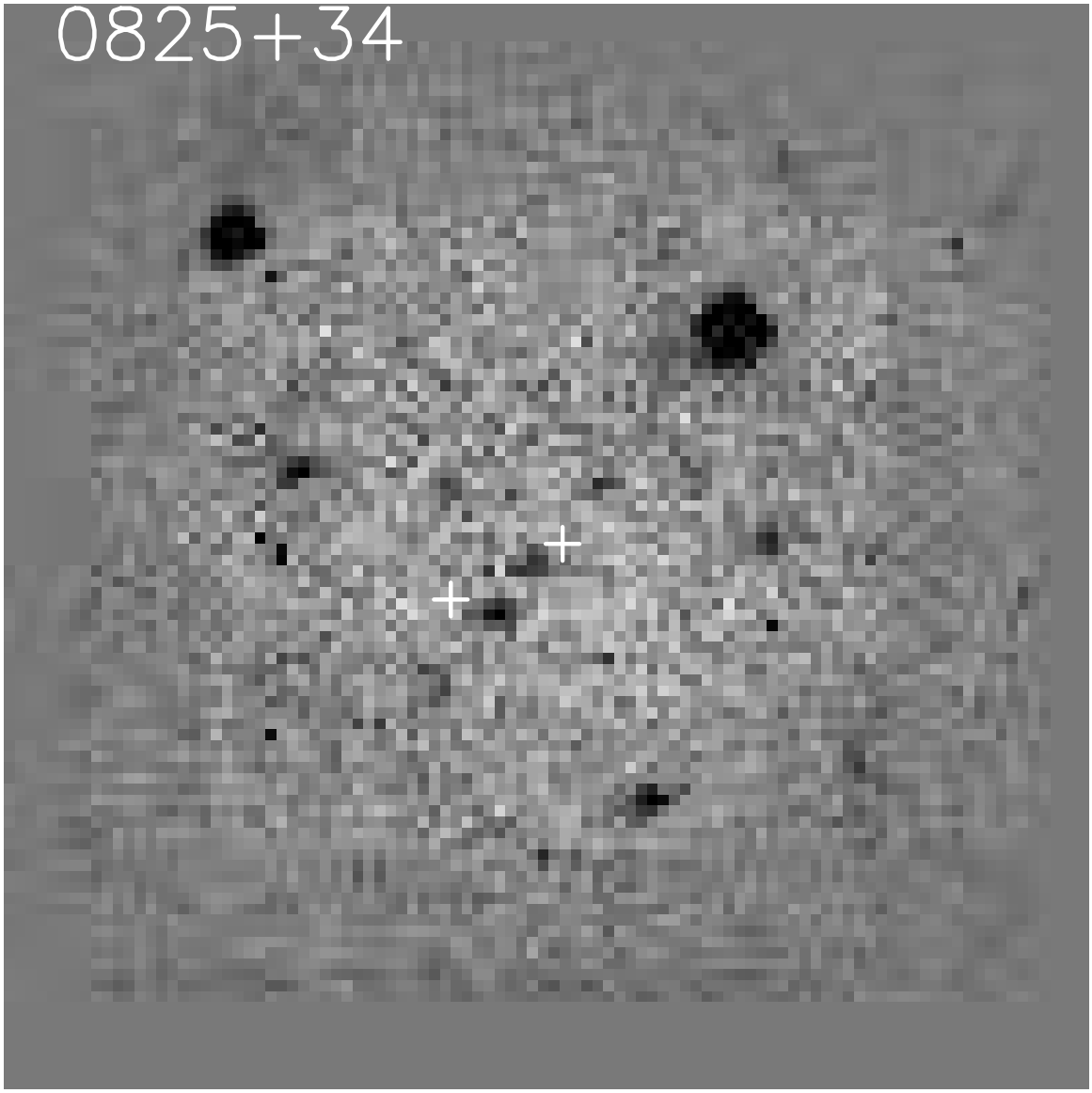
0825+34

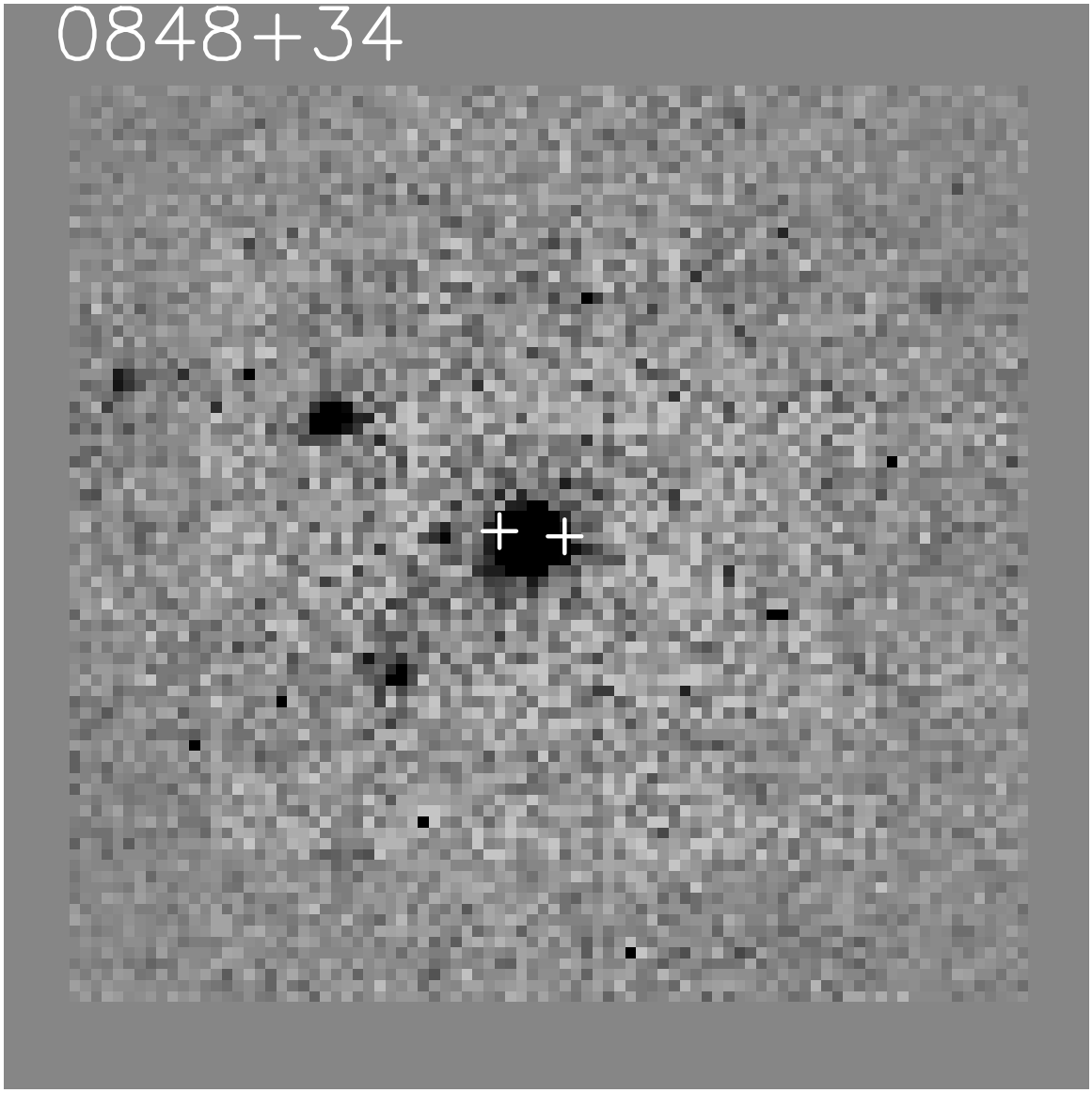
0848+34

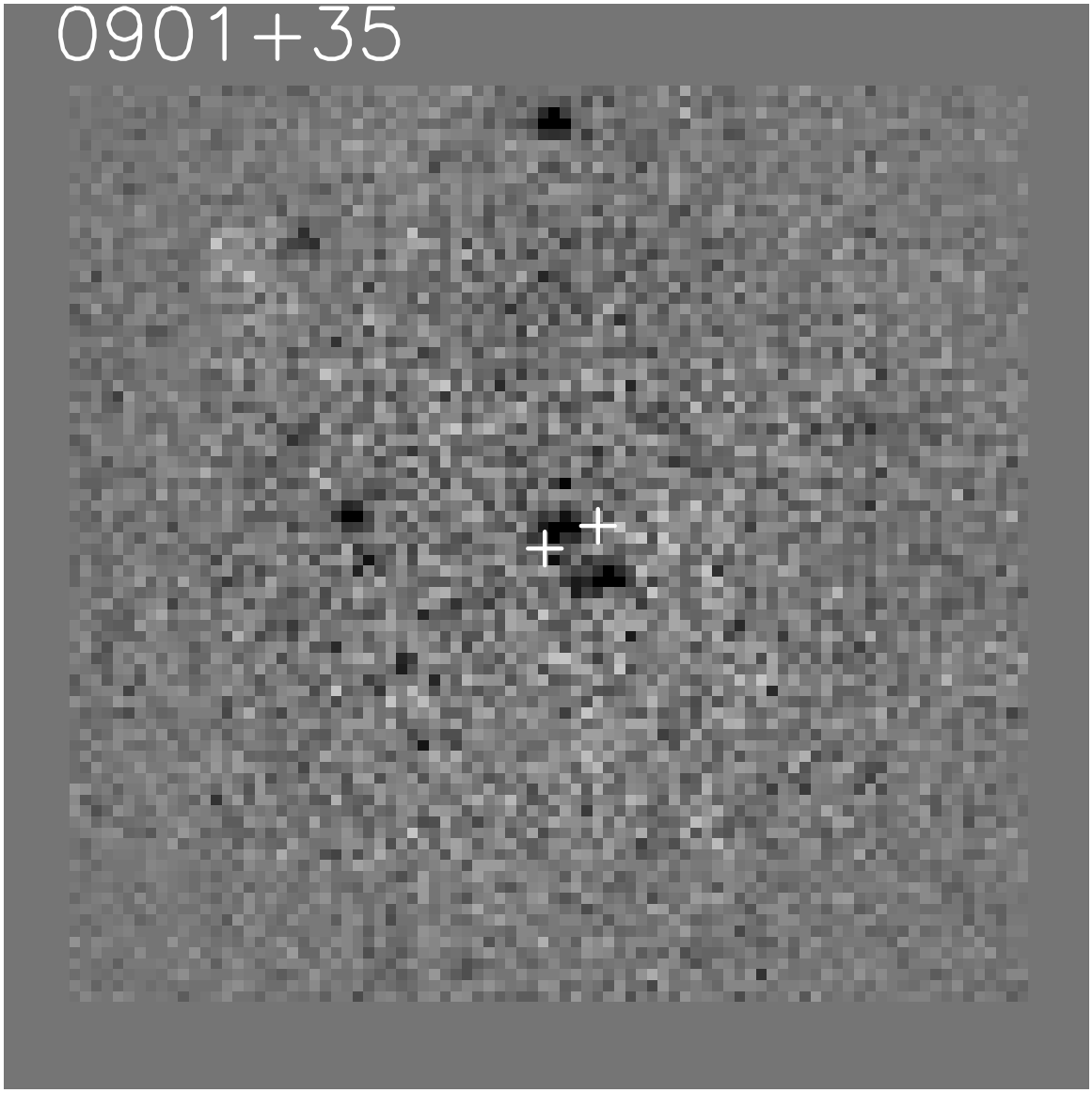
0901+35

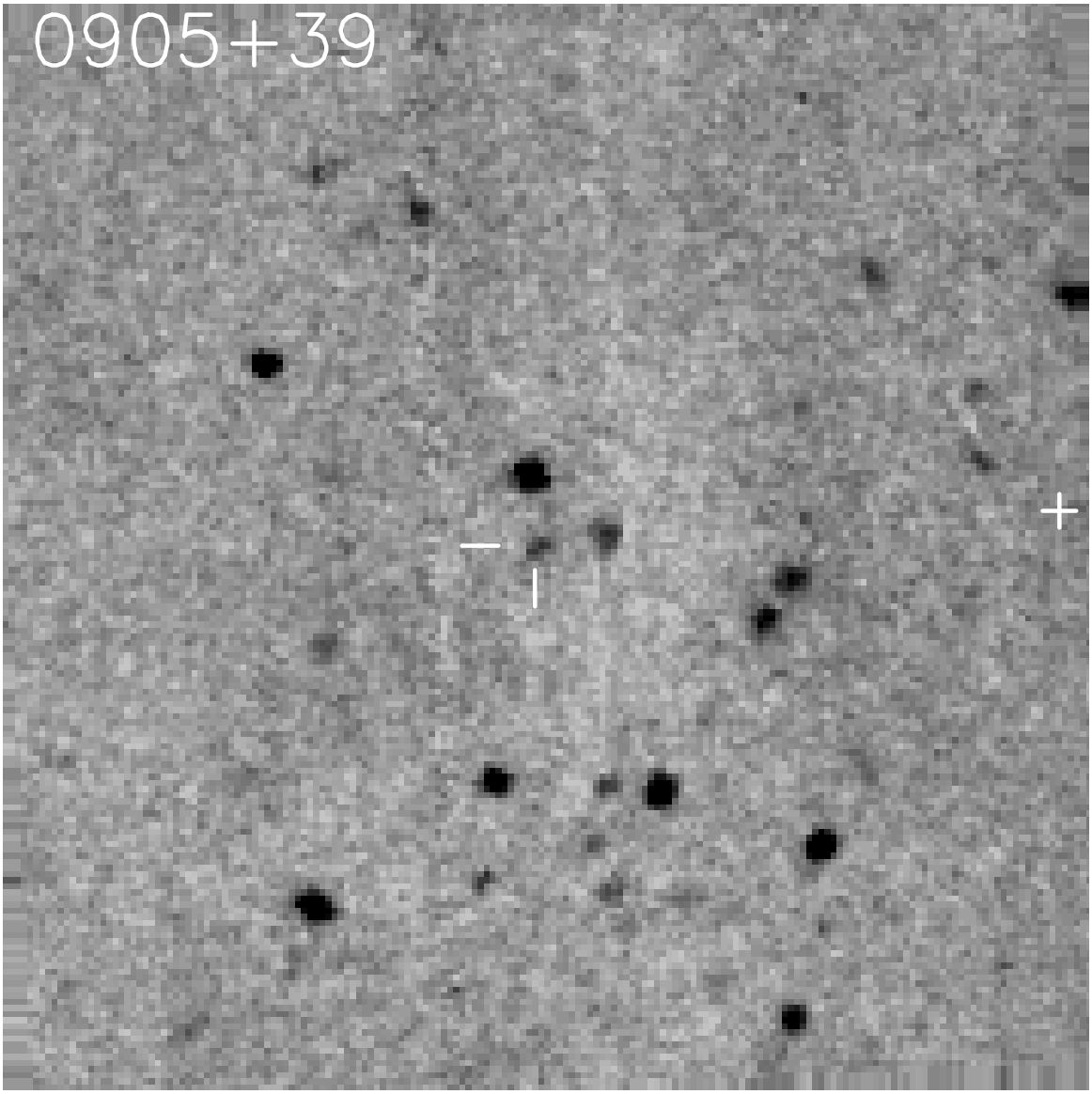
0905+39

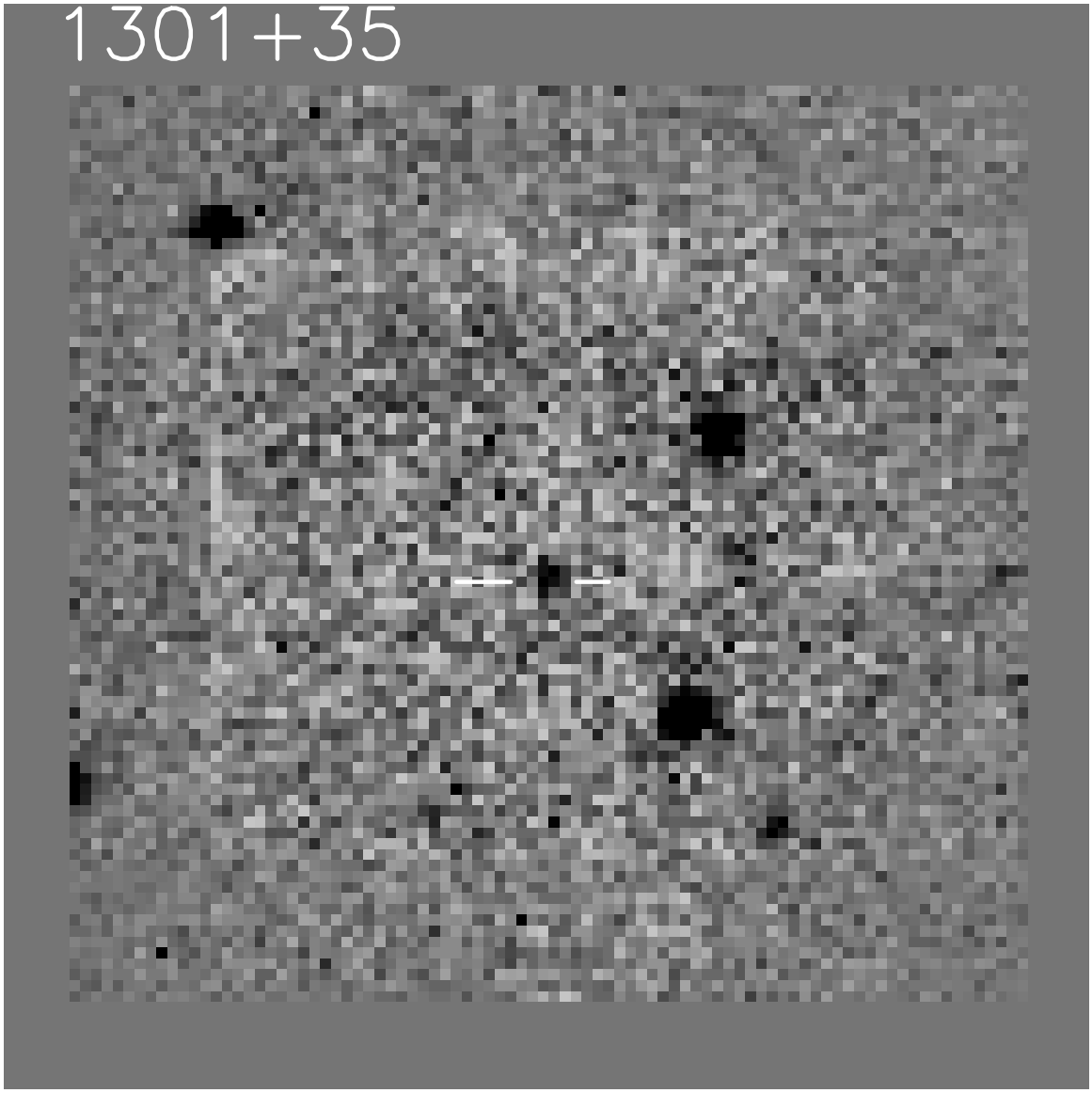
1301+35

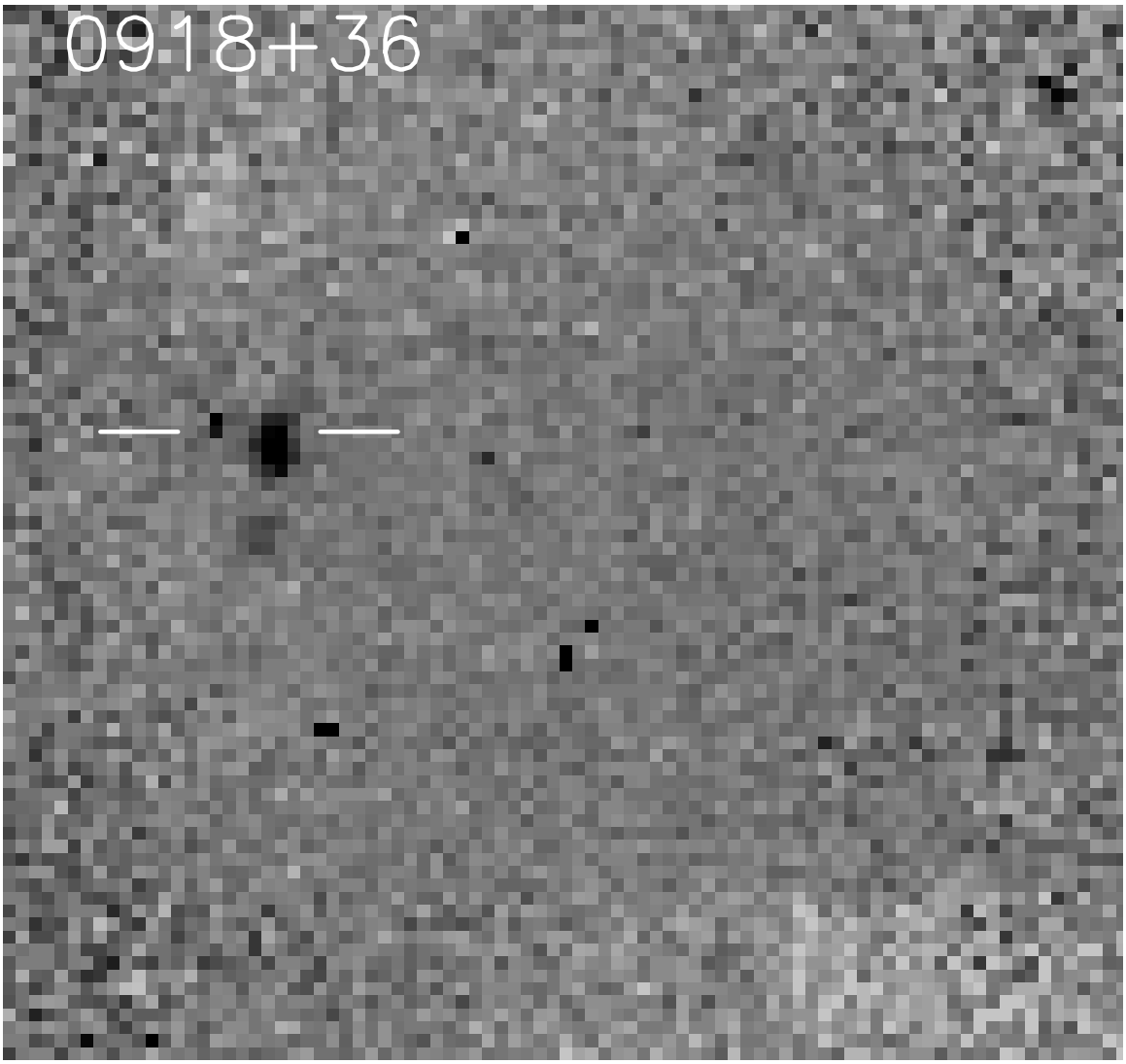
0918+36

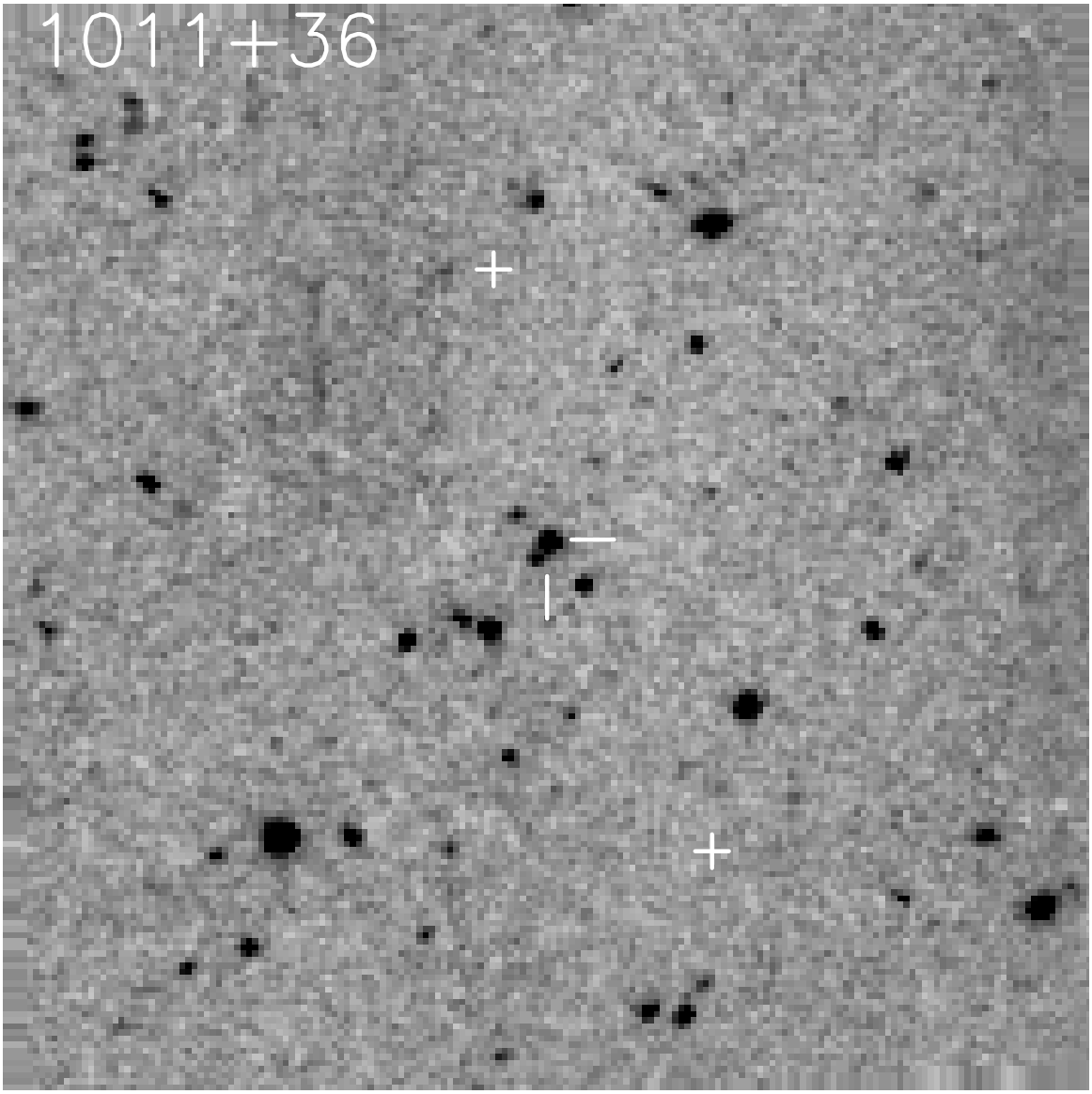
1011+36

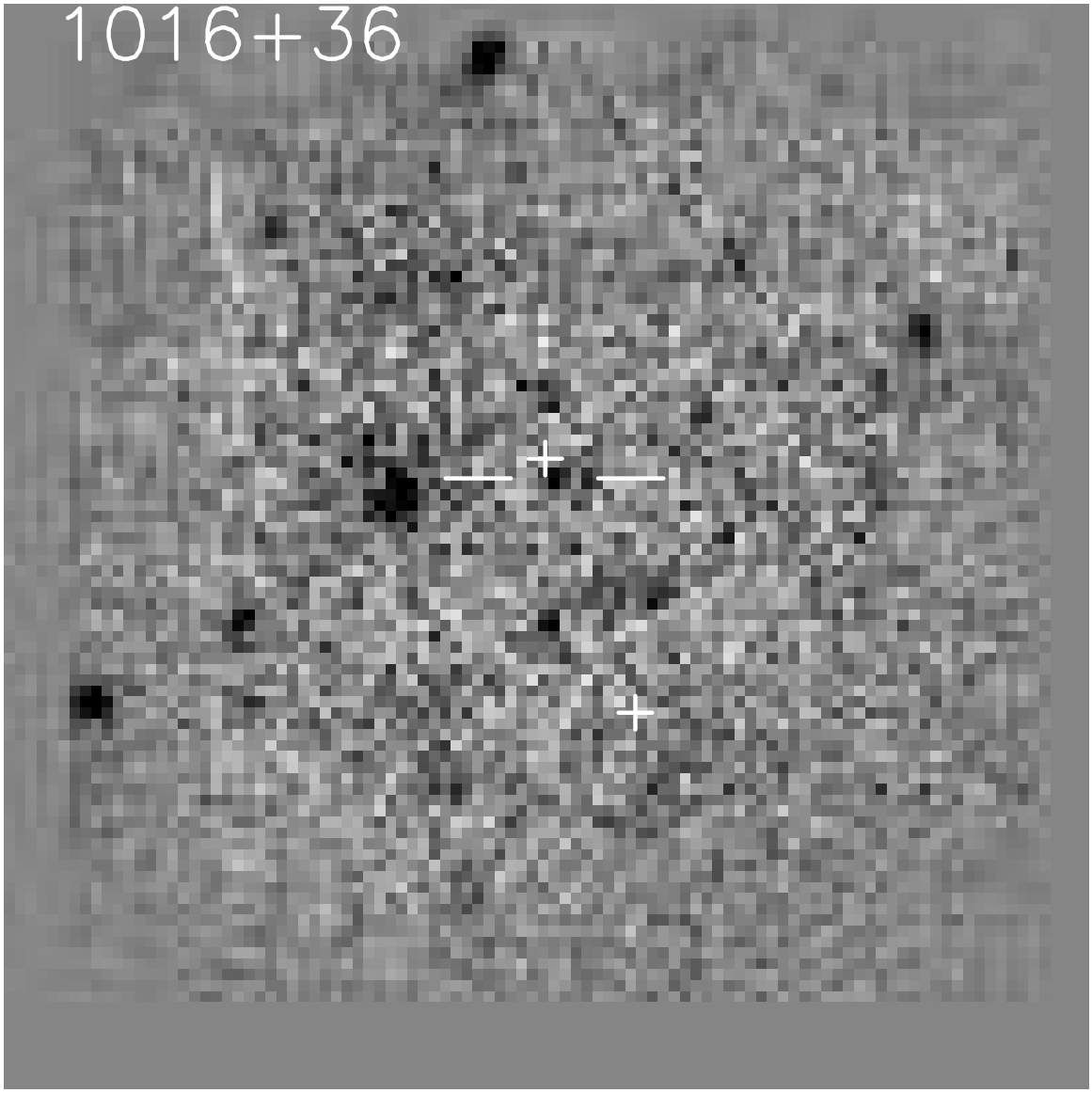
1016+36

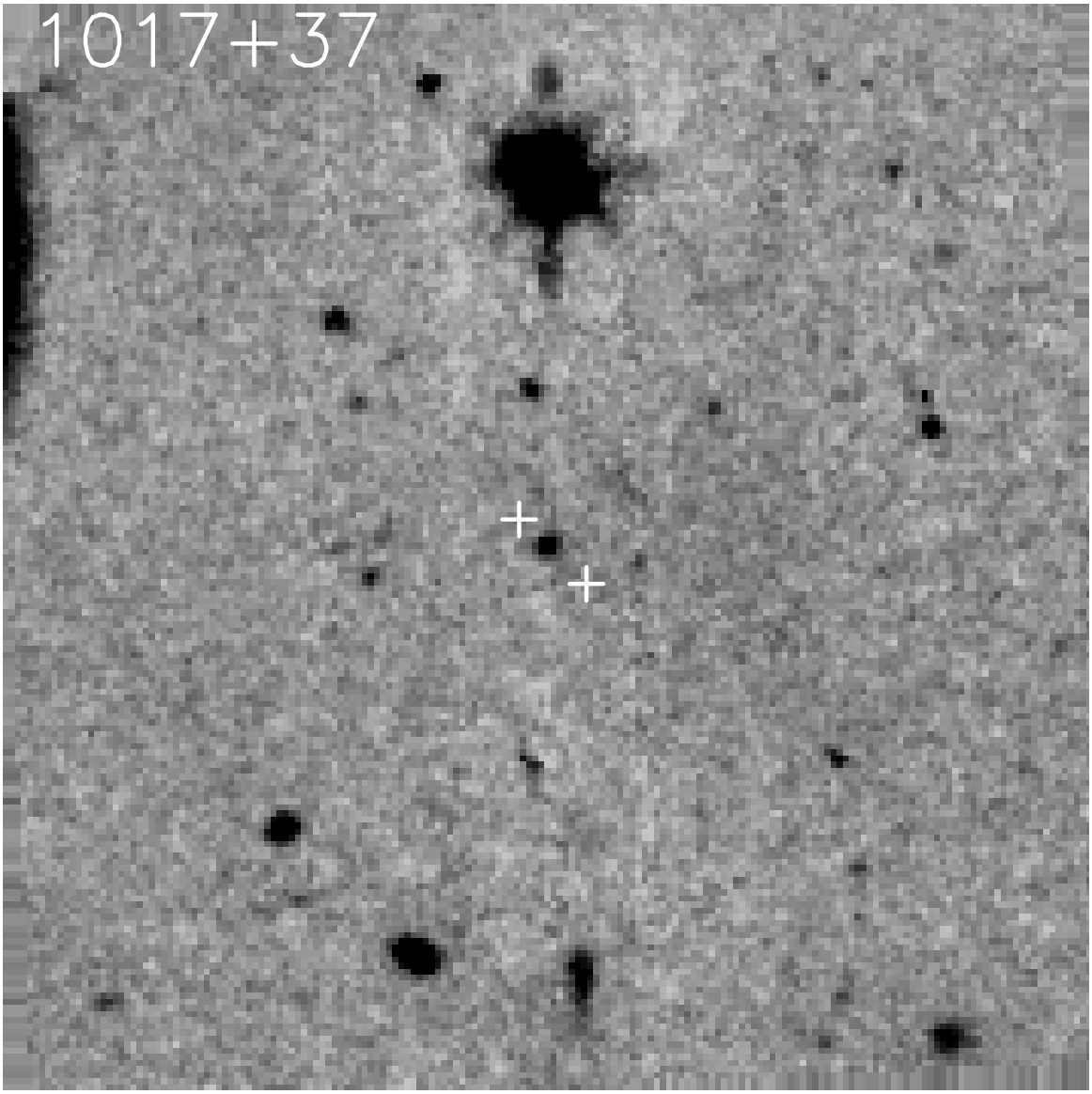
1017+37

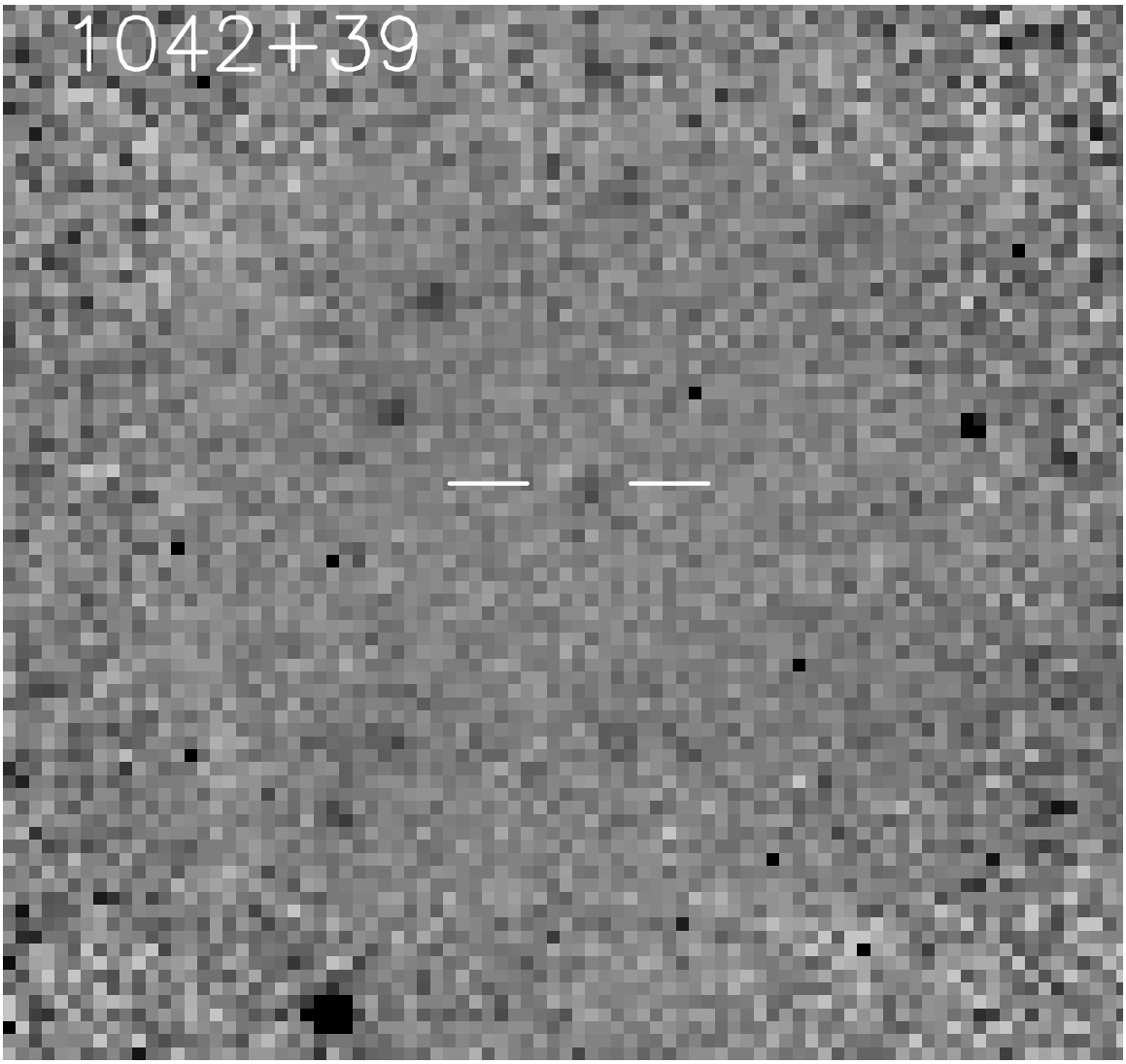
1042+39

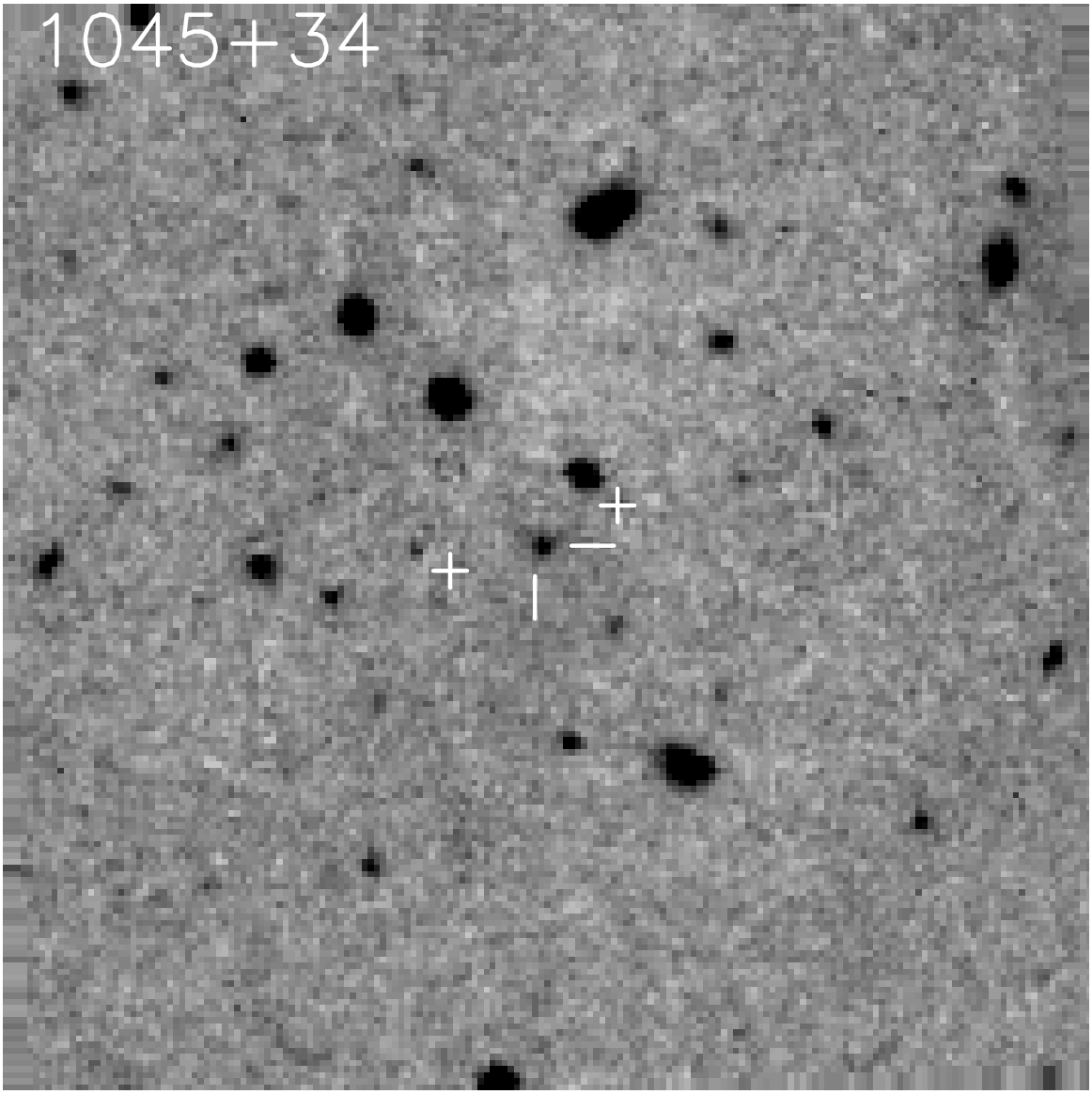
1045+34

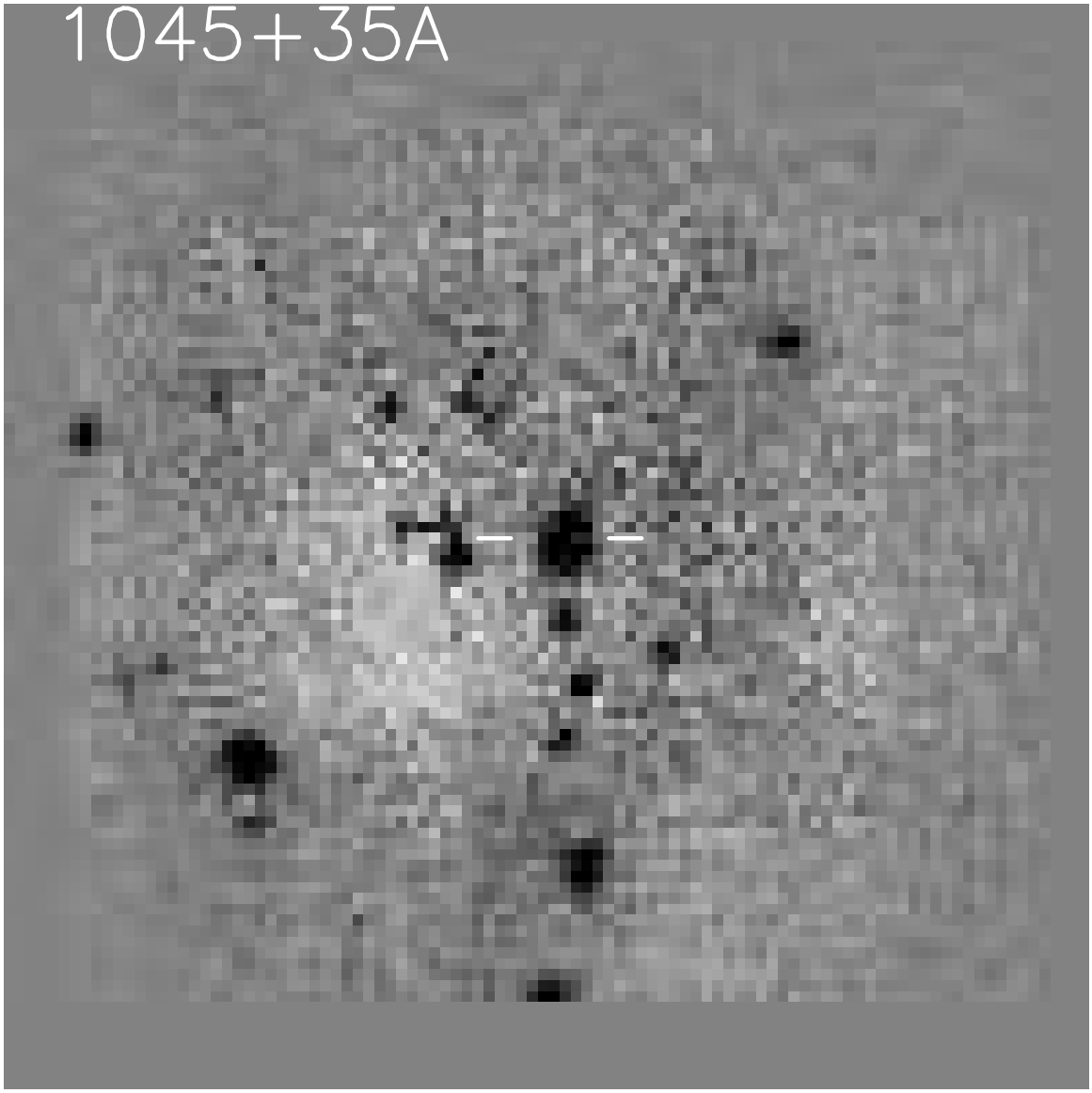
1045+35A

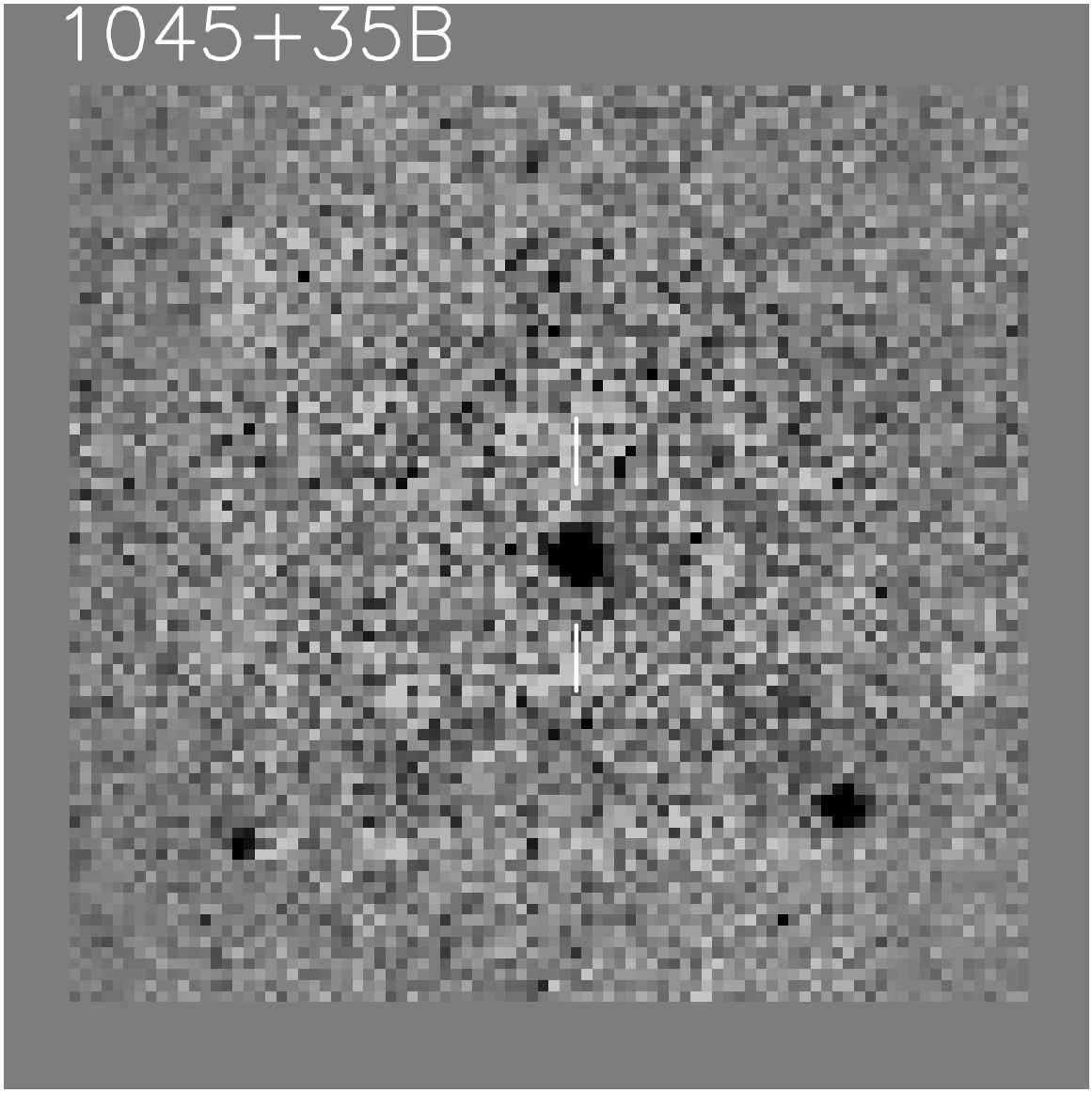
1045+35B

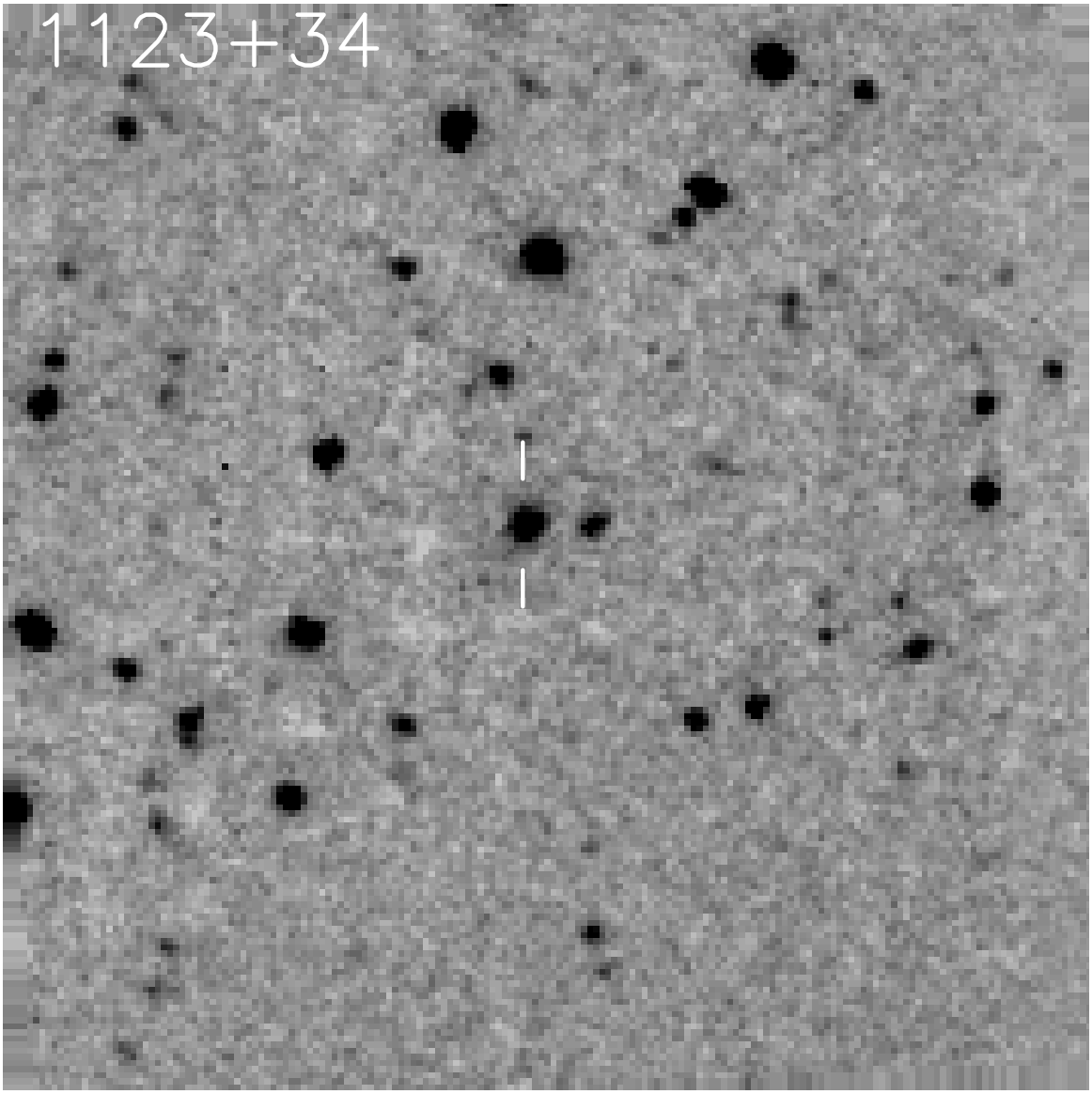
1123+34

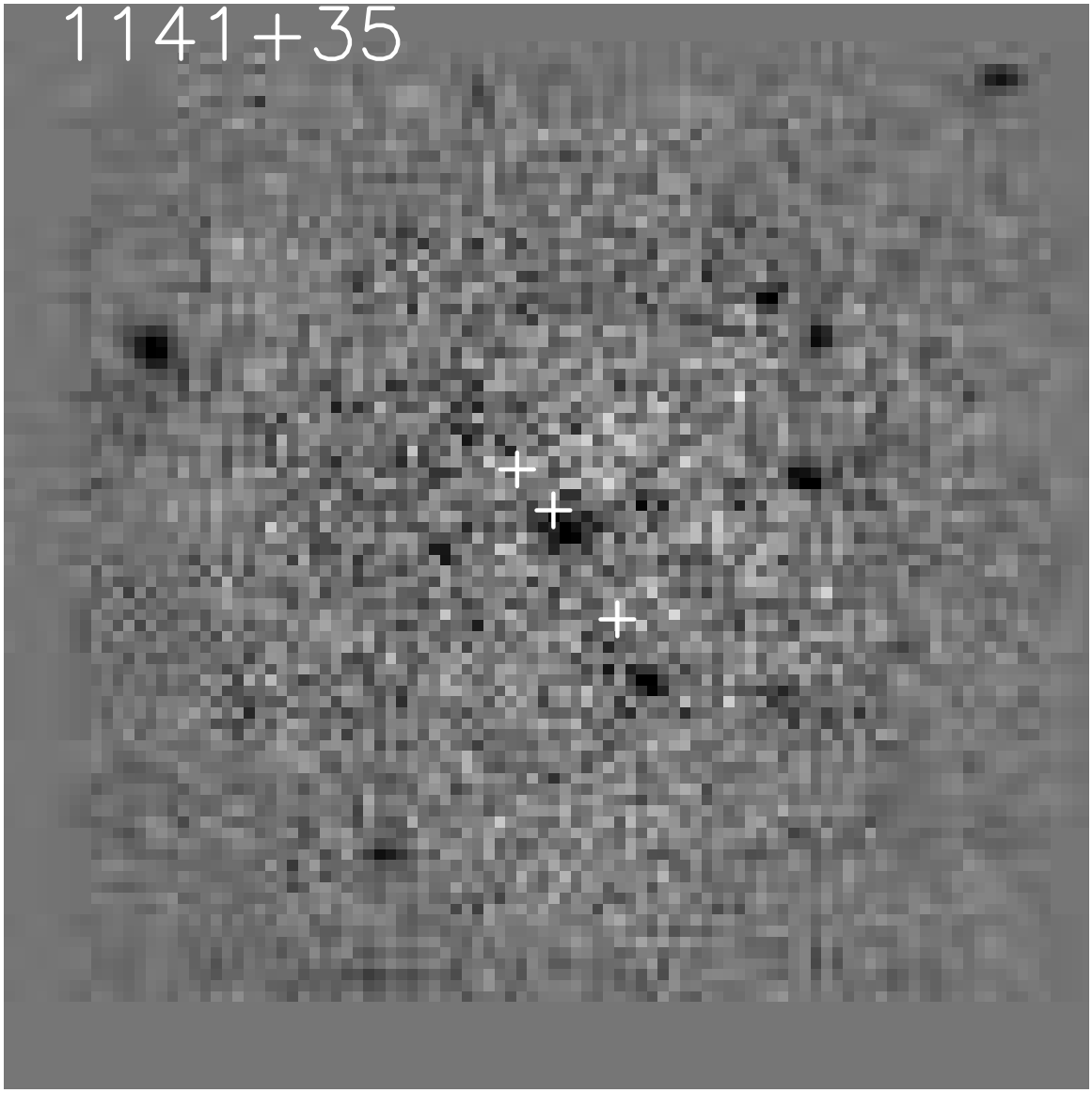
1141+35

1143+37

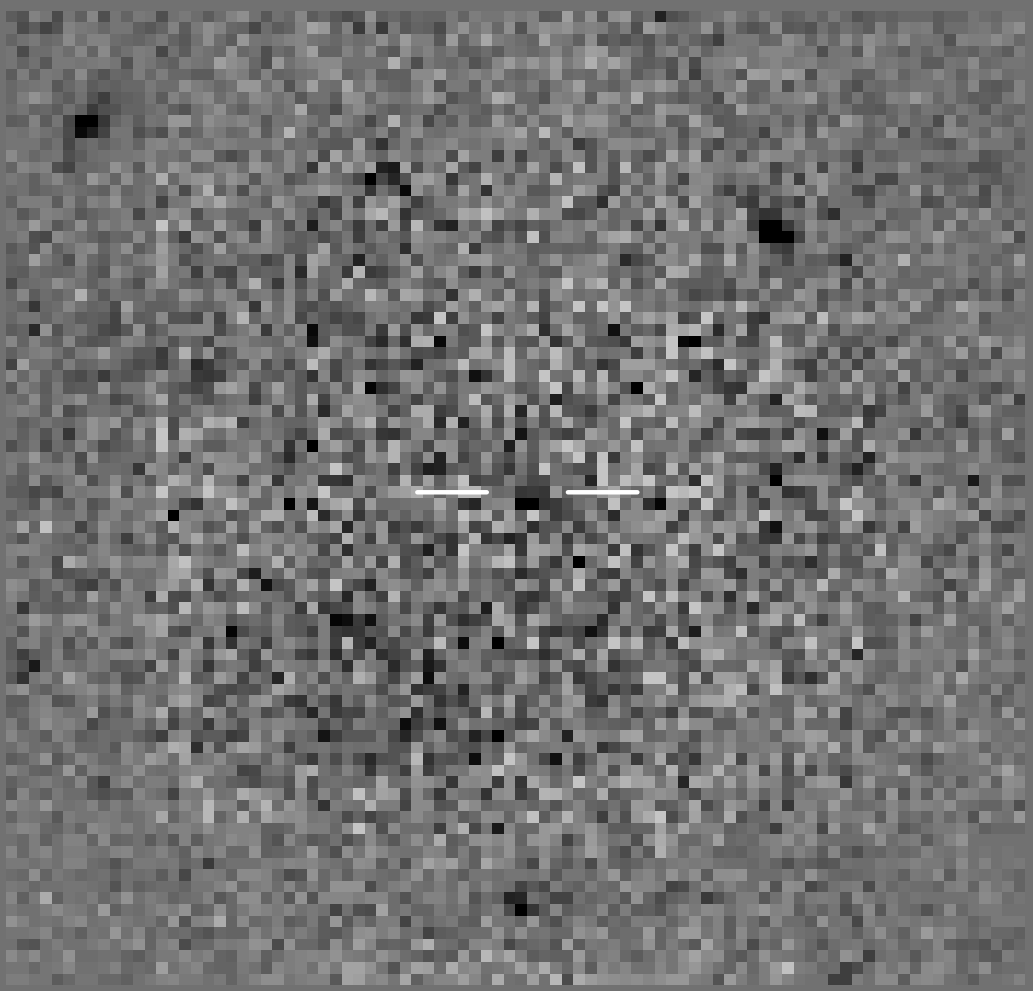

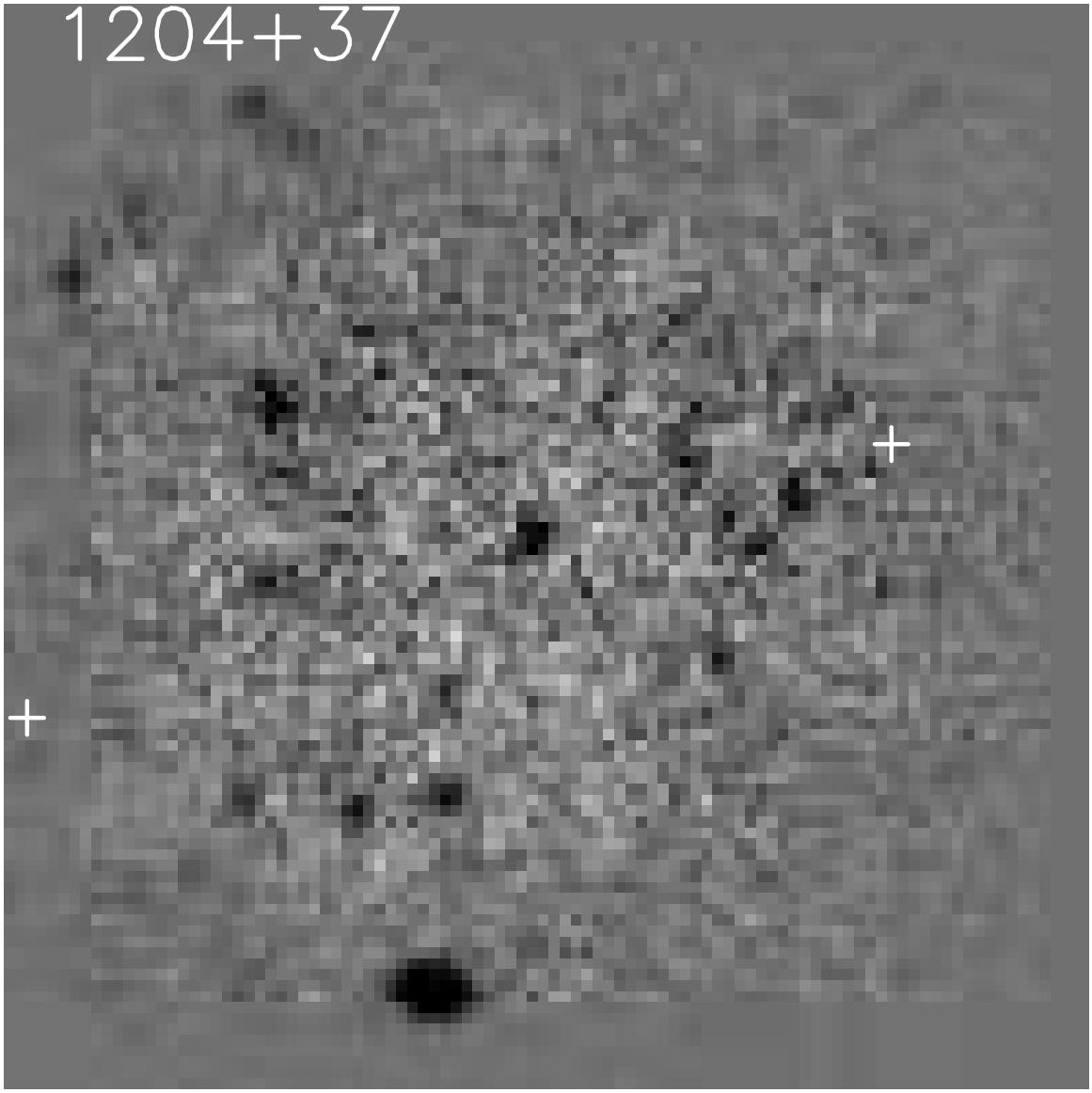
1204+37

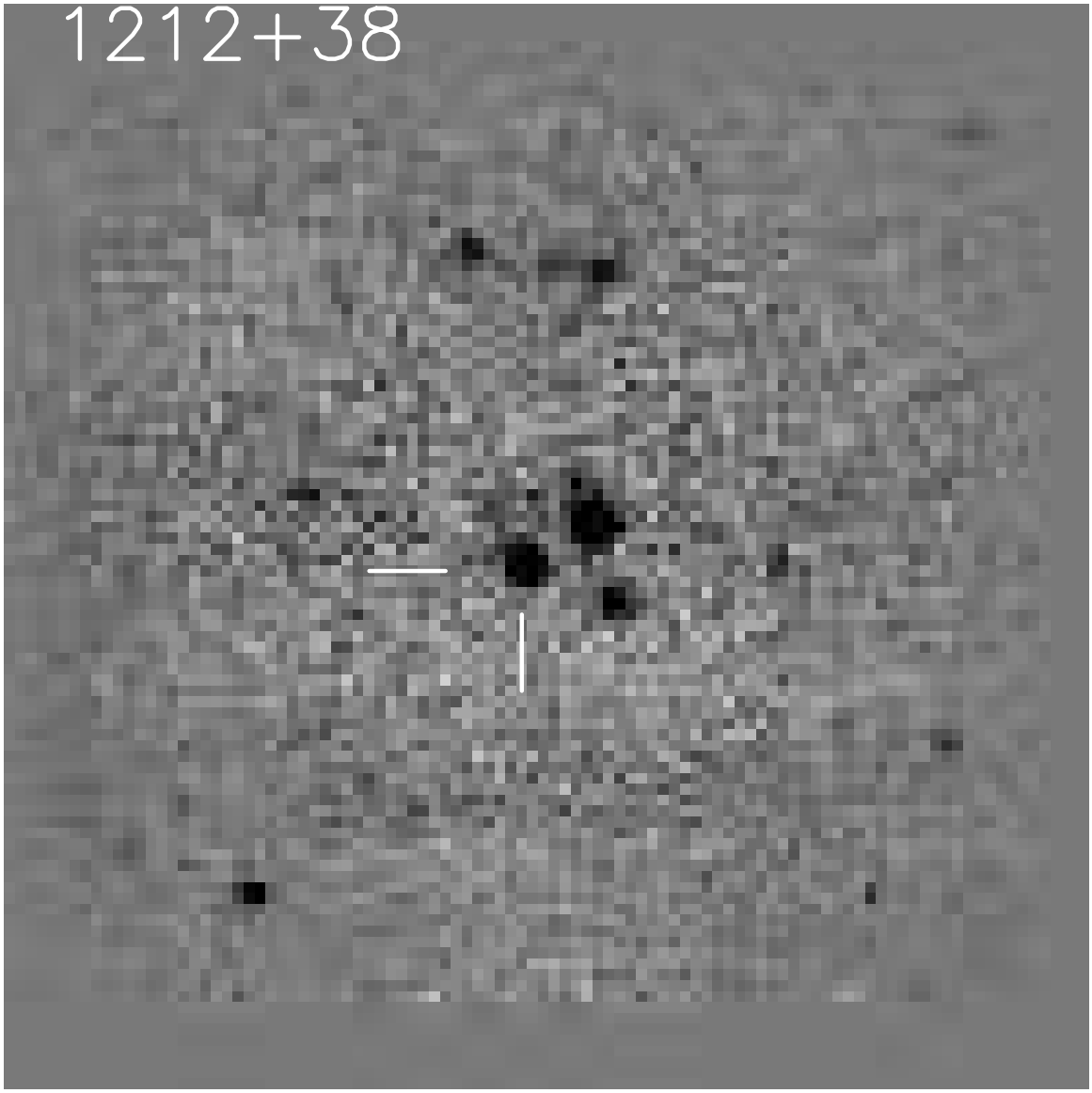
1212+38

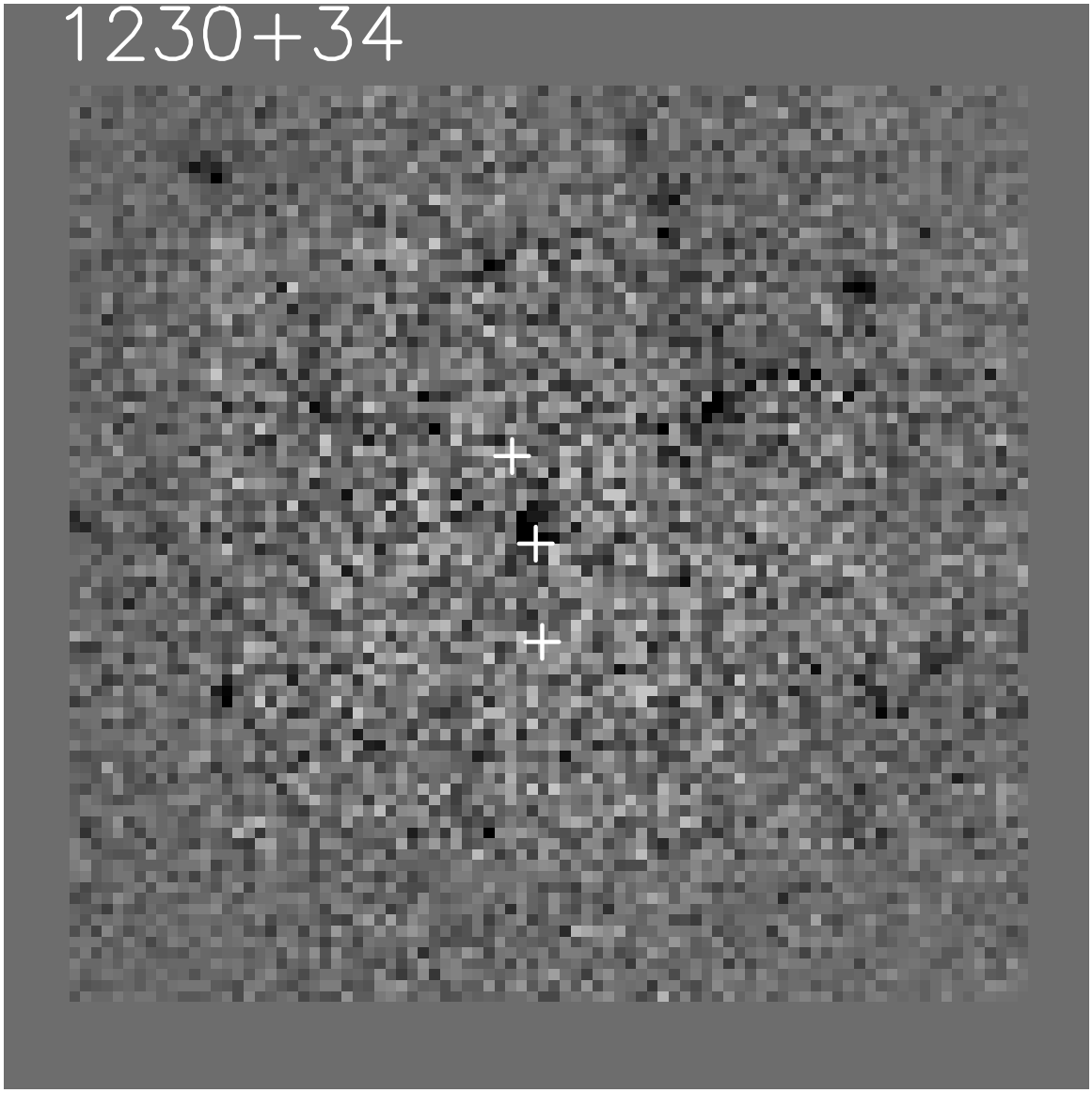
1230+34

(1) Name	(2) IRCAM(5)	(3) IRCAM(8)	(4) IRCAM3(5)	(5) IRCAM3(8)	(6) Red(5)	(7) Red(8)
0820+36 SW	19.00 ± 0.26	18.40 ± 0.25	...	...	...	...
0820+36 NE*	18.41 ± 0.16	18.16 ± 0.21	...	...	...	...
0822+34B NW	18.27 ± 0.13	17.57 ± 0.12	...	...	...	...
0822+34B SE*	17.71 ± 0.09	17.33 ± 0.10	...	...	...	...
0822+39	...	...	...	...	17.30 ± 0.06	17.22 ± 0.06
0825+34 NW	19.19 ± 0.21	18.51 ± 0.19	...	...	...	...
0825+34 SE*	19.00 ± 0.18	18.47 ± 0.19	...	...	...	...
0848+34	15.83 ± 0.06	15.70 ± 0.06	...	...	...	...
0901+35 SW	18.48 ± 0.17	18.15 ± 0.21	...	...	...	...
0901+35 NE*	18.29 ± 0.14	17.60 ± 0.13	...	...	...	...
0905+39	18.48 ± 0.17	...	...	...	19.11 ± 0.12	...
0918+36	16.88 ± 0.14	16.52 ± 0.22	...	...	...	...
0943+39	18.01 ± 0.09	17.94 ± 0.13	18.09 ± 0.09	17.95 ± 0.13	18.13 ± 0.12	18.13 ± 0.13
1011+36	18.05 ± 0.14	17.90 ± 0.20	...	...	17.73 ± 0.06	17.51 ± 0.07
1016+36	$(20.3^{+0.3}_{-0.2})$	...	...	...	...	...
1017+37	18.88 ± 0.19	18.85 ± 0.29	...	...	18.54 ± 0.12	18.29 ± 0.13
1042+39	$(19.7^{+0.5}_{-0.3})$	...	...	...	...	...
1045+34	18.91 ± 0.17	...	...	...	18.93 ± 0.08	...
1045+35A	16.33 ± 0.06	16.30 ± 0.07	...	...	...	...
1045+35B	16.77 ± 0.06	16.63 ± 0.07	...	...	...	...
1100+35	...	...	18.33 ± 0.27	...	...	...
1123+34	17.92 ± 0.11 ...	...	...	17.81 ± 0.11	17.75 ± 0.12	...
1129+37	...	...	17.52 ± 0.06	17.31 ± 0.07	17.43 ± 0.06	17.34 ± 0.07
1141+35	18.72 ± 0.14	...	...	...	...	...
1143+37‡	$(19.83^{+0.56}_{-0.37})$	...	...	...	...	...

1204+37	19.29 ± 0.13	...	...	...	...	...	...
1204+35	...	...	17.97 ± 0.07	17.72 ± 0.10	17.88 ± 0.06	17.79 ± 0.07	(17
1212+38 NW	17.44 ± 0.06	17.15 ± 0.07	...	...	...	...	...
1212+38 SE*	17.74 ± 0.07	17.35 ± 0.08	...	...	...	...	...
1217+36	...	...	17.27 ± 0.05	17.02 ± 0.06	17.28 ± 0.11	17.17 ± 0.12	(17
1230+34	18.40 ± 0.14	18.25 ± 0.21	...	...	...	...	...
1256+36	...	...	17.75 ± 0.06	17.60 ± 0.08	17.52 ± 0.06	17.10 ± 0.06	17.
1257+36	17.51 ± 0.08	17.43 ± 0.11	...	...	17.58 ± 0.12	17.36 ± 0.12	...
1301+35	$(19.46^{+0.35}_{-0.27})$	...	...	...	...	...	18.

The format of this table is as follows. Col. (1) gives the name of the object or the component of the object. If there are two component listed, there are two objects in the infrared image close to the radio position (Fig. 2). The asterisk indicates the component we have concluded is the site of the active nucleus. Cols (2)-(7) give the magnitudes measured with IRCAM, IRCAM3 and REDEYE. The name at the head of each column gives the instrument with which the object was observed and the number in brackets is the diameter in arcsec through which the magnitude was measured, unless there are brackets around the magnitude itself—in which case the diameter of the aperture used was 4 arcsec. Col. (8) gives the magnitude measured either by Lilly (1989) or by Lilly, Longair & Allington-Smith (1985). This was measured through an aperture of diameter 8 arcsec, unless the magnitude is in brackets—in which case the aperture had a diameter of 12 arcsec.

‡ The object is significant at the 2.6σ level.

Fig. 3

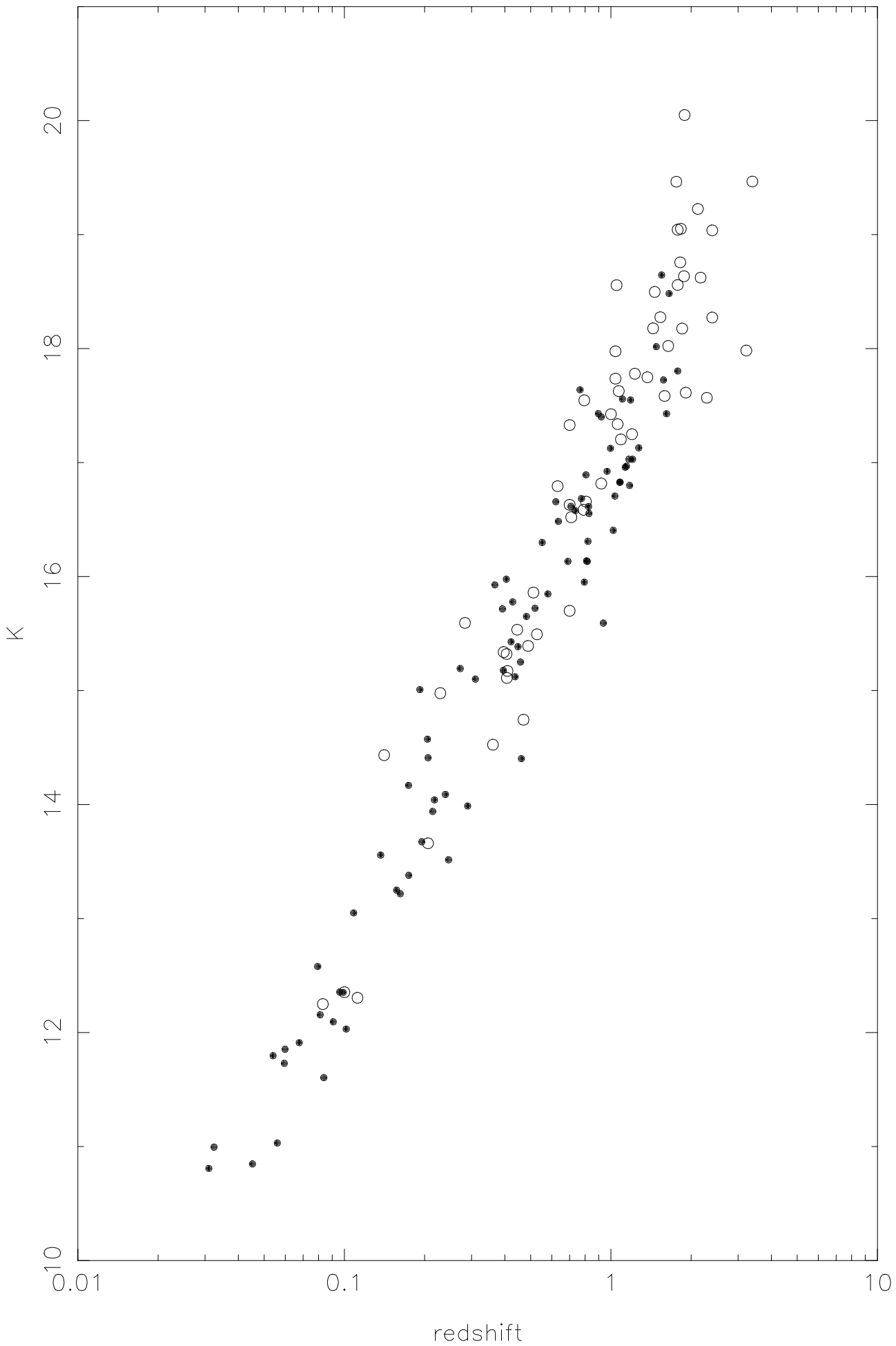

(1) Name	(2) Position (1950.0)	(3) Core?	(4) Radio reference	(5) Position reference
0820+36	08 20 33.92 36 42 28.4	Yes	1	a
0822+34B	08 22 36.51 34 34 16.2	Yes	1	a
0822+39	08 22 05.51 39 29 33.6	Yes	1	b
0825+34	08 25 15.96 34 52 45.3	No	1,2	a
0848+34	08 48 00.68 34 30 41.6	No	2	a
0901+35	09 01 25.02 35 51 01.8	No	2	a
0905+39	09 05 04.95 39 55 34.8	Yes	1,3	a
0918+36	09 18 06.27 36 17 52.9	No	1	c
0943+39	09 43 13.93 39 58 10.9	No	2	a
1011+36	10 11 16.89 36 32 12.2	Yes	1,2	a
1016+36	10 16 58.45 36 37 49.7	No	1,2	d
1017+37	10 17 44.7 37 12 08	No	1,2	b
1042+39	.....	No	2	...
1045+34	10 45 24.20 34 03 37.1	Yes	1	a
1045+35A	10 45 41.59 35 53 53.0	Yes	2	e
1045+35B	10 45 45.82 35 13 17.1	Yes	2	e
1100+35	11 00 40.89 35 05 56.9	Yes	1	b
1123+34	11 23 43.16 34 01 56.8	Yes	2	a
1129+37	11 29 55.29 37 10 52.0	No	1	f
1141+35	11 41 13.72 25 25 00.8	No	1,2	a
1143+37	.....	Yes	1,2	...
1204+37	12 04 21.75 37 08 20.0	No	1	a
1204+35	12 04 59.37 35 19 46.8	Yes	1	f
1212+38	12 12 26.15 38 05 31.1	Yes	2	a
1217+36	12 17 40.13 36 45 45.5	Yes	1,2	f
1230+34	12 30 13.97 34 59 22.5	Yes	1	a
1256+36	12 56 44.75 36 48 08.4	No	1	b
1257+36	12 57 08.87 36 33 13.4	No	1	a
1301+35	13 01 32.70 35 25 55.2	Yes	1	b

The format of the table is as follows: Col. 1—IAU name of source; col. 2—Position (1950.0) of the optical or infrared identification. The accuracy of these positions is discussed in the text (§2.2). Col. 3—A yes in this column indicates that the radio source either has a core or a compact radio structure. Col. 4—References for radio maps. The reference key is as follows: 1—Law-Green et al. (1995a); 2—Naundorf et al. (1992); 3—Law-Green et al. (1995b). Col.

6—Reference for the optical or infrared position. The key is as follows: a—this paper; b—Lilly (1989); c—unpublished measurement from a CCD image (Eales, unpublished); d—unpublished measurement from a CCD image (Allington-Smith, private communication); e—Eales (1985b); f—Allington-Smith et al. (1982).

Fig. 4

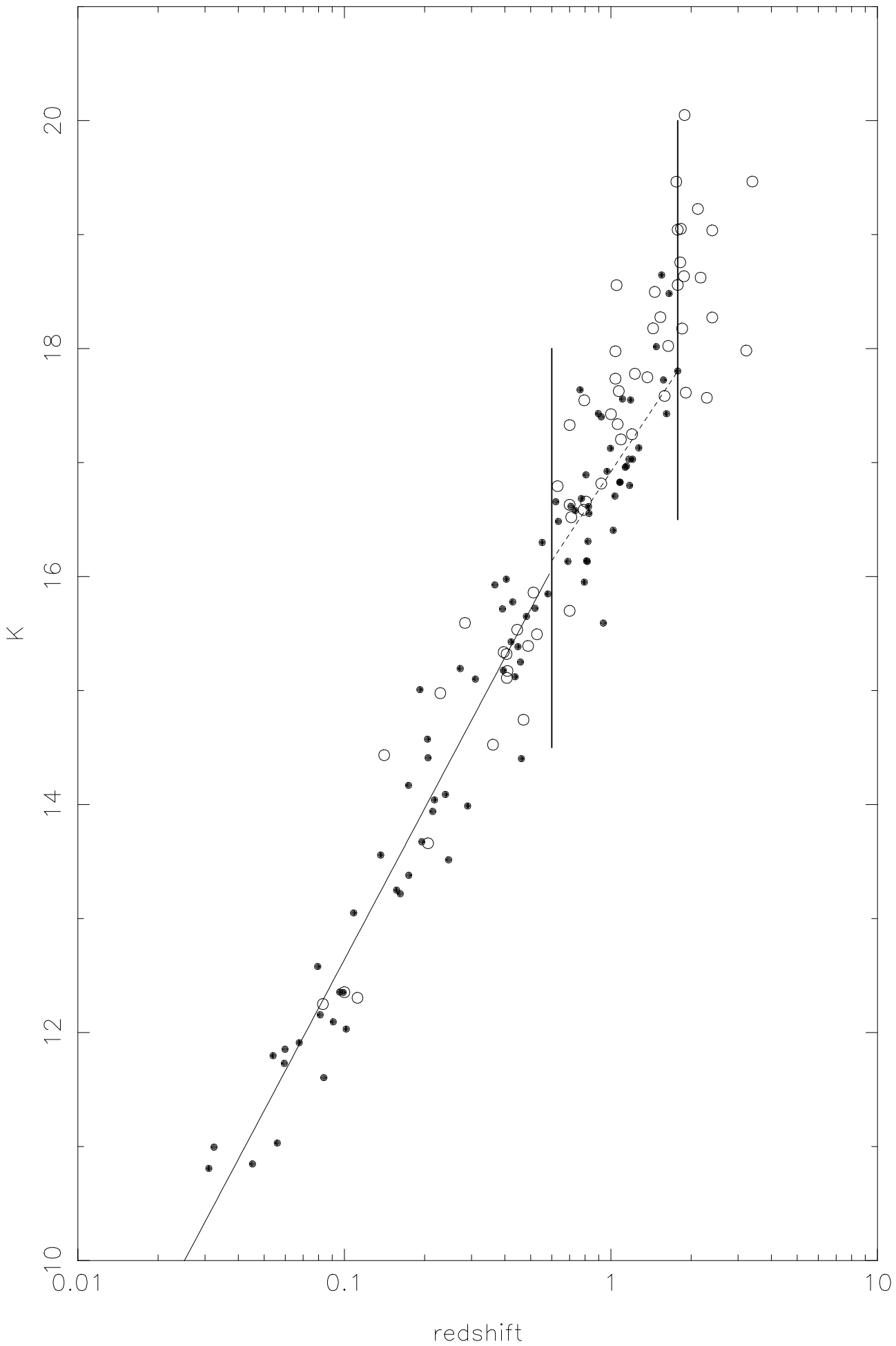

(1) Name	(2) Redshift	(3) Angular size (arcsec)	(4) Radio P.A.	(5) K-band P.A.
0825+34	1.46	6.9	117.4	152.5
0943+39	1.04	10.6	100.3	99.5
1011+36	1.04	50.7	20.6	45.0
1017+37	1.05	7.6	46.3	54.5
1100+35	1.44	13.2	81.6	154
1129+37	1.06	14.0	137.6	100.0
1204+35	1.37	16.3	12.1	13.5
1256+36	1.07	15.5	48.1	98.5
1257+36	1.00	38.5	139.8	97.5

The format of the table is as follows: Col. 1—IAU name of source; col. 2—redshift; col. (3)—angular size of radio source in arcsec; col. (4)—radio position angle measured in degrees east of north; col. (5)—K-band position angle measured in degrees east of north.

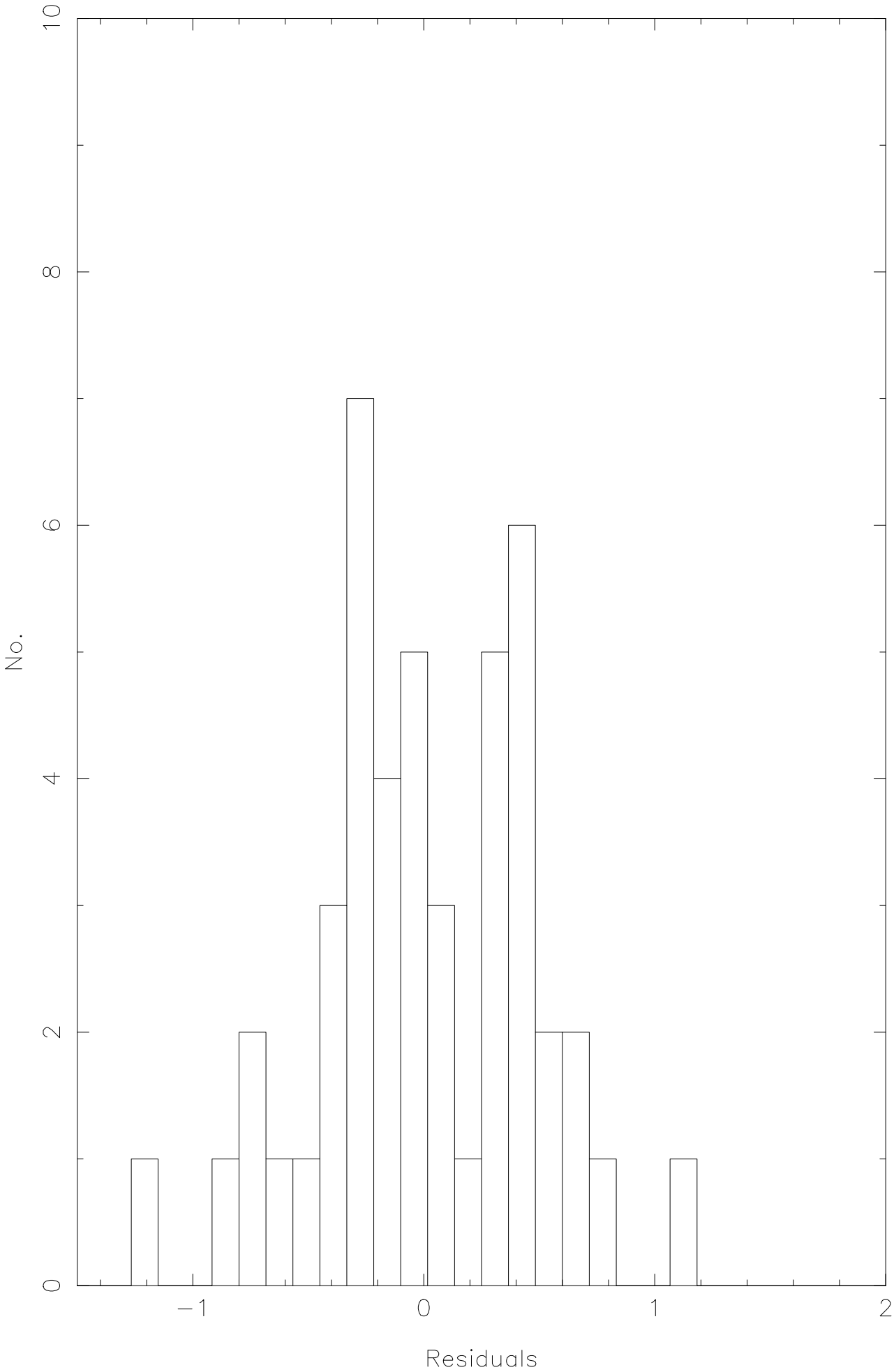
No.
0
2
4
6
8
10
−1
0
1
2
Residuals

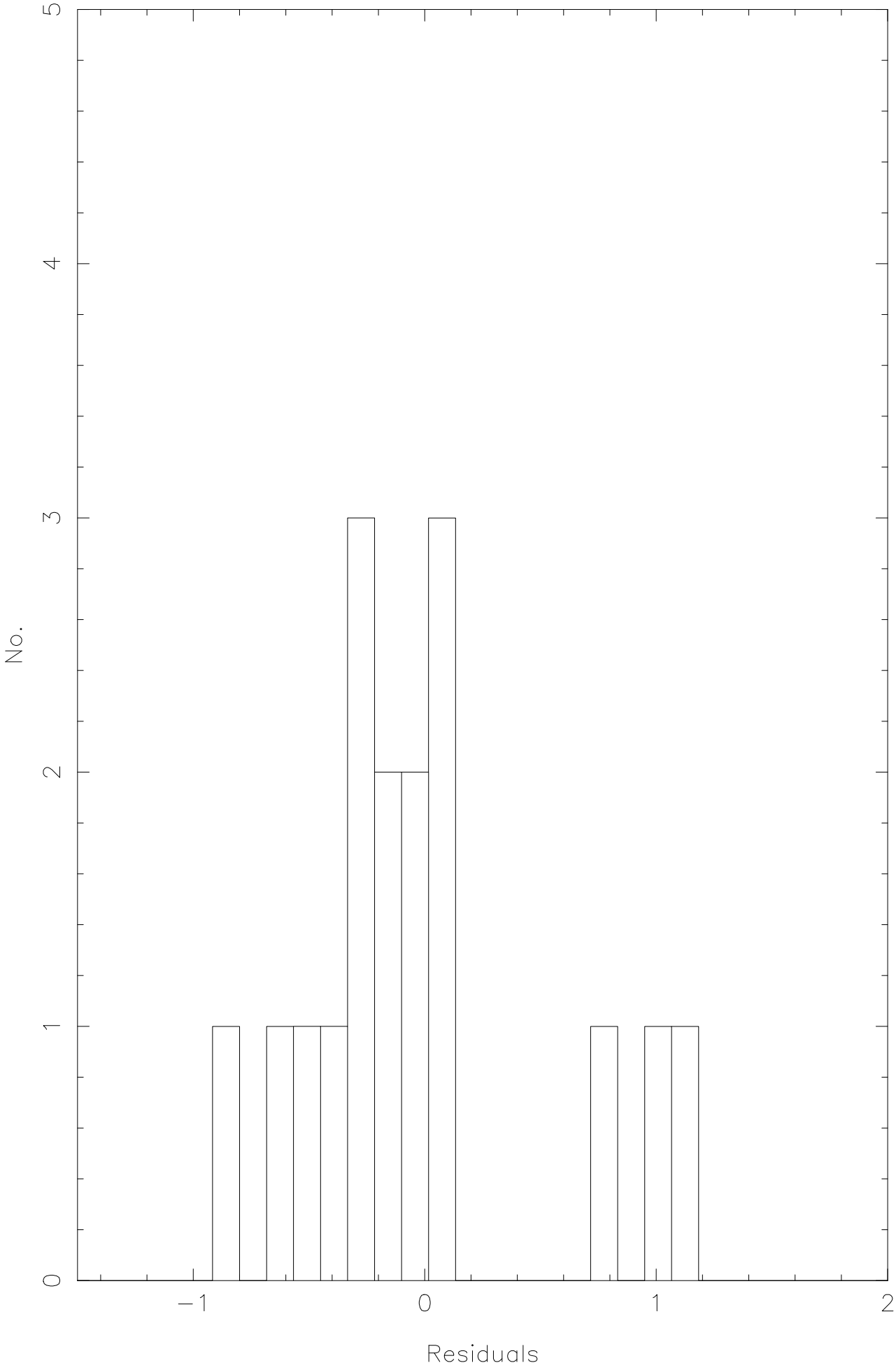
No.
0
1
2
3
4
5
−1
0
1
2
Residuals

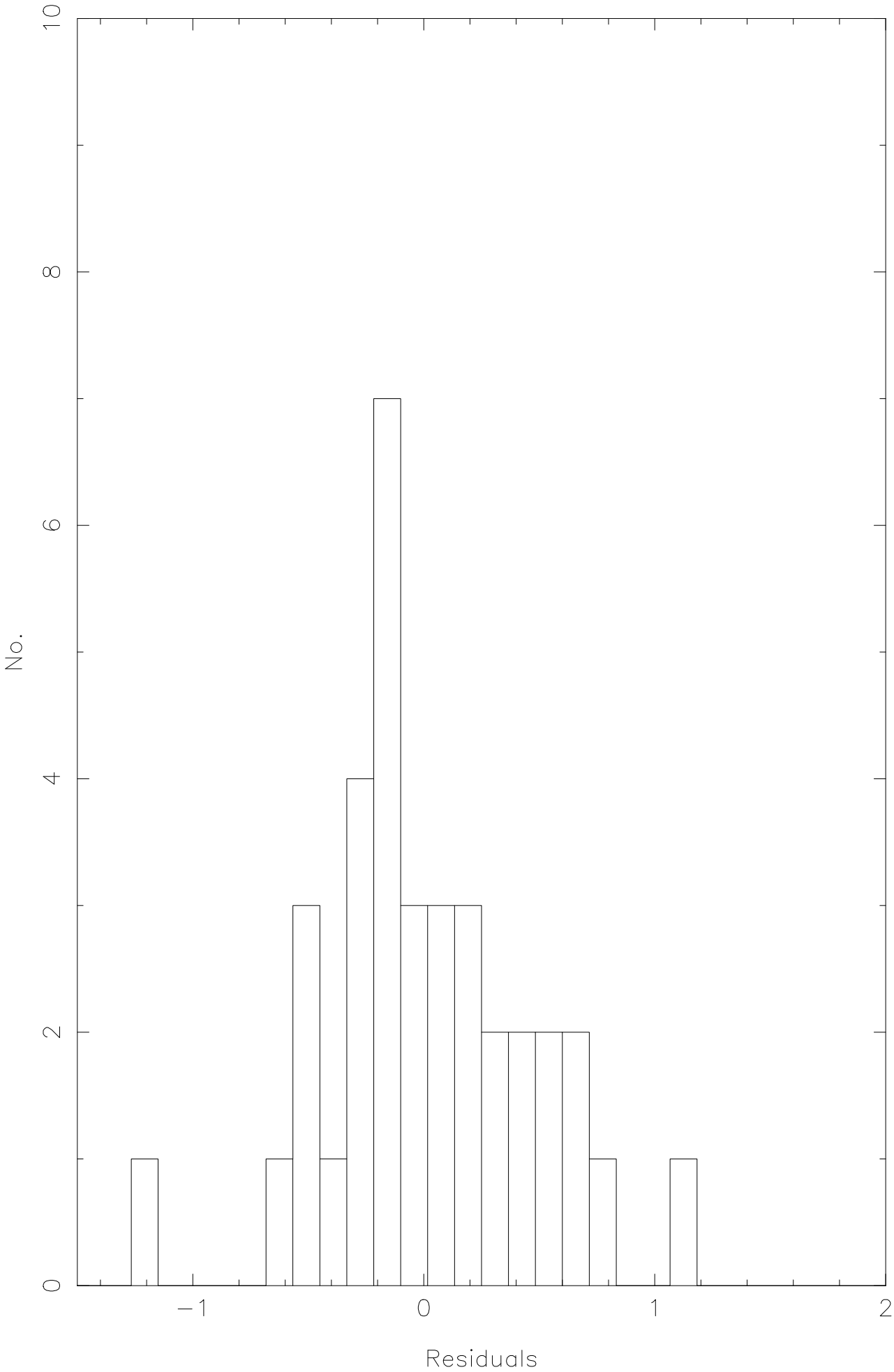
No.
0
2
4
6
8
10
−1
0
1
2
Residuals

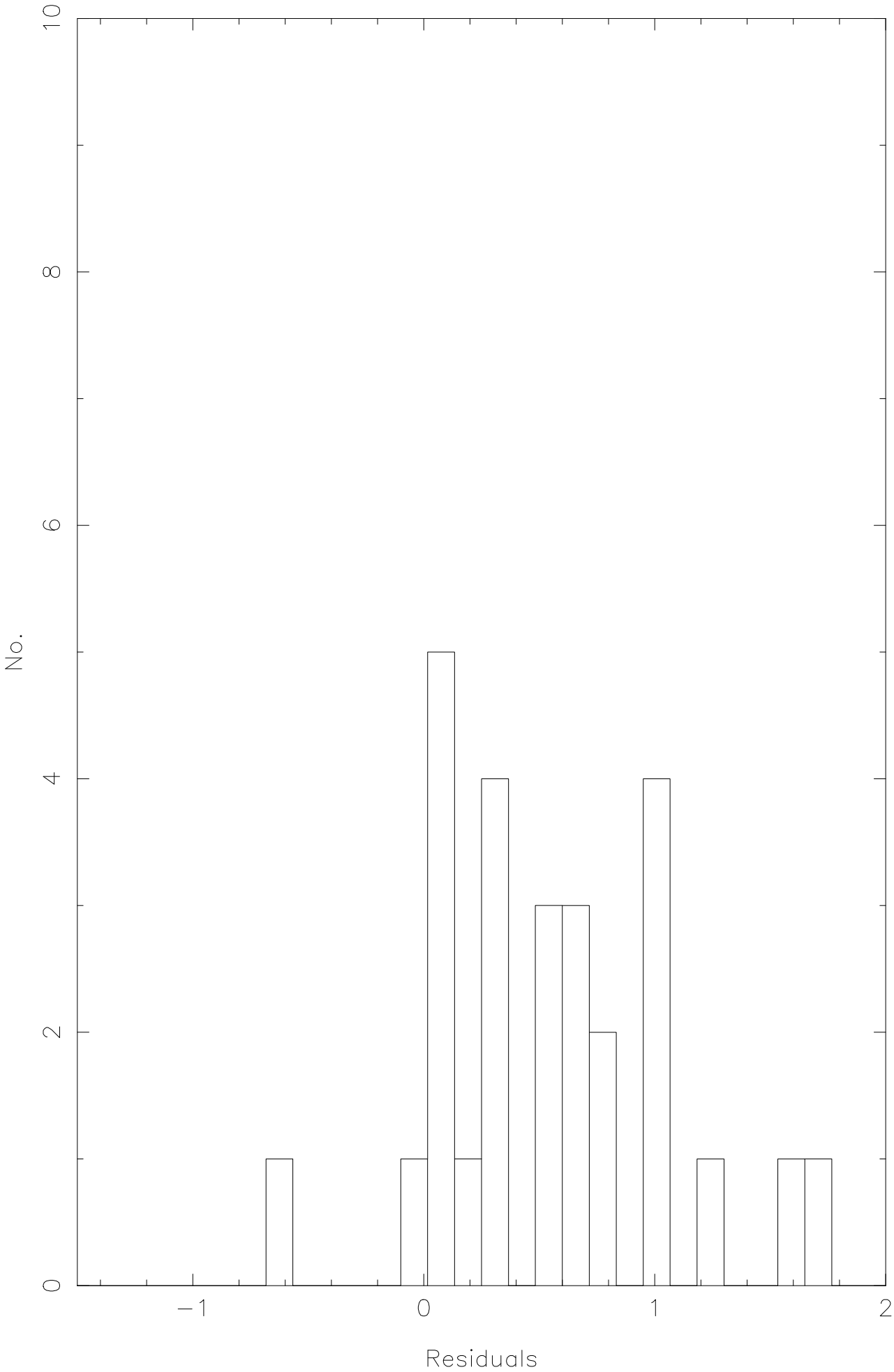
No.
0
2
4
6
8
10
−1
0
1
2
Residuals

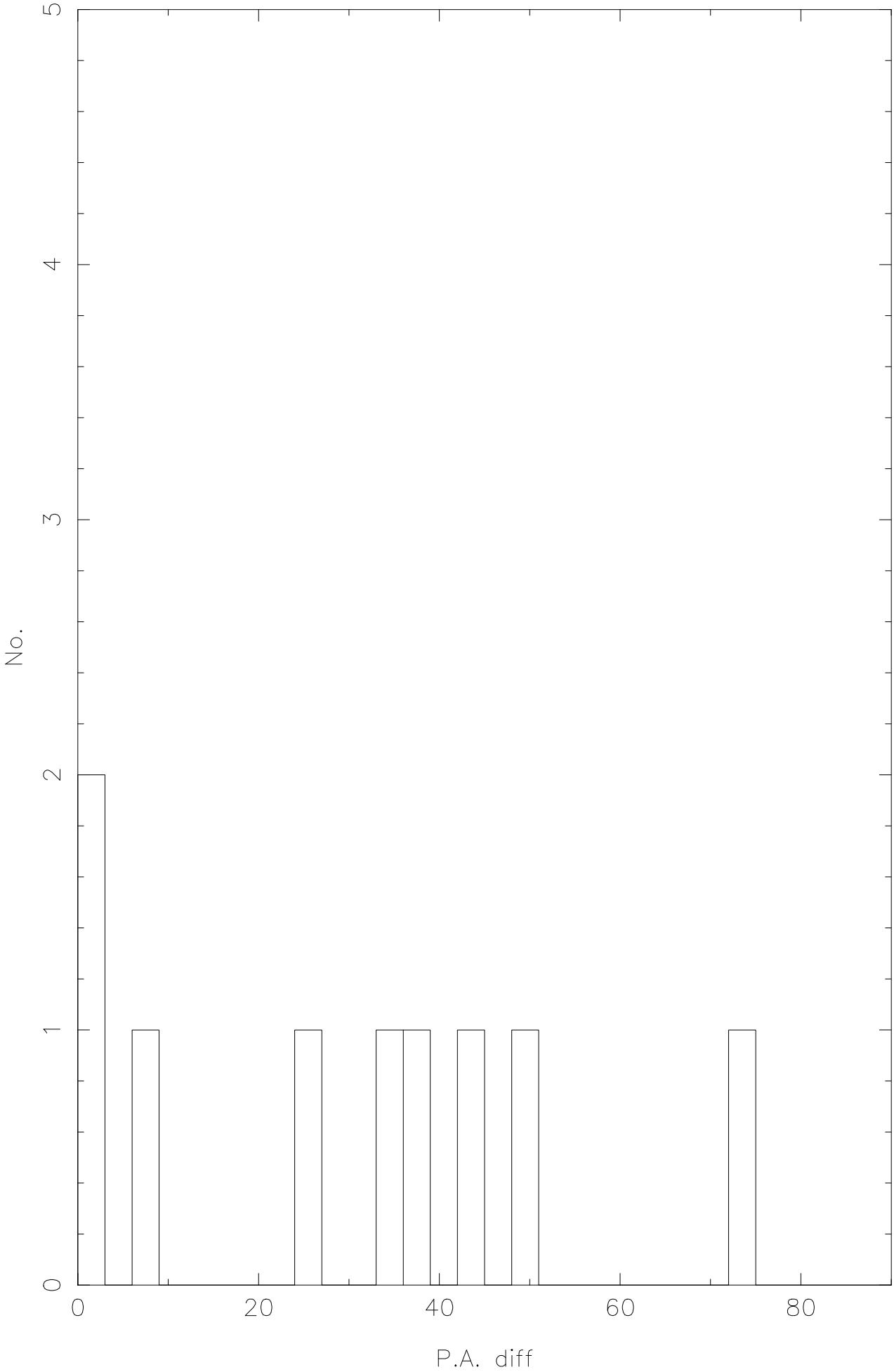
No.
0
1
2
3
4
5
0
20
40
60
80
P.A. diff

A first sample of faint radio sources with virtually complete redshifts I. Infrared images, the Hubble diagram, and the alignment effect

Stephen Eales[1], Steve Rawlings[2], Duncan Law-Green[4], Garret Cotter[3] and Mark Lacy[2]

1 Department of Physics and Astronomy, University of Wales Cardiff, P.O. Box 913, Cardiff CF2 3YB

2 Department of Astrophysics, University of Oxford, Nuclear and Astrophysics Laboratory, Keble Road, Oxford, OX1 3RH

3 Mullard Radio Astronomy Observatory, Cavendish Laboratory, Madingley Road, Cambridge CB3 0HE

4 Nuffield Radio Astronomy Laboratories, Jodrell Bank, Macclesfield, Cheshire SK11 9D11

Abstract

We have obtained redshifts and infrared images for a sample of faint B2/6C radio sources whose fluxes are about six times fainter than those of sources in the bright 3C sample. We now have unambiguous redshifts for 90% of the sources, making this the first faint radio sample with such complete redshift information. We find that the infrared Hubble diagrams (K versus z) of the 3C sample and the B2/6C sample are similar at a low redshift ($z < 0.6$), but by a redshift of $z \sim 1$ the 6C/B2 galaxies are on average $\simeq$0.6 mags fainter in the K-band than 3C galaxies at the same redshift. This suggests that the bright K-magnitudes of 3C galaxies at $z \sim 1$ are not the result of stellar evolution, but of a correlation between infrared and radio luminosity. We also find that the infrared stuctures of B2/6C galaxies at $z \sim 1$ are less clearly aligned with their radio structures than 3C galaxies at this redshift, implying that the strength of the alignment effect depends on radio luminosity. Finally, above a redshift of 2 we find that the dispersion in the K-z relation of the B2/6C sample is $\simeq 2.7$ times greater than that at low redshift, a result which is expected if at these redshifts we are beginning to penetrate into the epoch in which radio galaxies formed.

1. Introduction

Radio galaxies appear very different at low and high redshifts. In the local universe radio galaxies are always giant elliptical galaxies with a small spread of absolute magnitude (Laing, Riley & Longair 1983). In the high-redshift universe the optical image of a typical radio galaxy consists of a series of knots strung out along the radio axis, nothing like the image expected for a giant elliptical, with the alignment suggesting a connection between the optical and radio emission (Chambers, Miley & van Breugel 1987; McCarthy et al. 1987; Longair, Best & Rottgering 1995). Other differences are that high-redshift radio galaxies (henceforth HZRG's) have brighter near-infrared magnitudes and bluer optical-infrared colours than are expected from the properties of their low-redshift counterparts (Lilly & Longair 1984), higher emission-line luminosities (Rawlings et al. 1989; Jackson & Rawlings 1996; Eales & Rawlings 1993, 1996), and smaller radio sizes (Eales 1985c); radio galaxies at high redshift are often surrounded by extensive ($D \sim 100$ kpc) line-emitting nebulae (McCarthy, van Breugel & Kapahi 1991) that are not seen around those at low redshift; and finally the optical emission from HZRG's is often polarised, with the electric vector perpendicular to the radio axis, again suggesting a connection between the radio and optical emission (Tadhunter et al. 1992).

It is tempting to attribute these differences to cosmic evolution. For example, a natural explanation of the brighter near-infrared magnitudes of HZRG's is the expected cosmic evolution of the stellar population of a radio galaxy. A present-day giant elliptical galaxy contains lots of stars but very little current star formation, suggesting that a large burst of star formation must have happened at some point in its past. If so, the galaxy should gradually have declined in brightness after the burst because of the evolution of the main-sequence turnoff mass. Lilly and Longair (1984) showed that the amount of evolution present in the radio galaxy K-z diagram is in agreement with detailed models of this effect. This was a very satisfying result because, as low-redshift radio galaxies do contain stars, it would have been surprising if the effects of stellar evolution had not been seen for radio galaxies at z $\sim$ 1, which for a universe with $\Omega_0 = 1$ is an epoch 65% of the way back to the beginning of the universe. The other differences can also be explained, although usually in a more ad hoc and often unsatisfactory way. The optical structures of HZRG's, for example, do look remarkably like simulations arising from models of galaxy formation based on hierarchical clustering (e.g. Fig. 3 of Baron & White 1987), but this does not explain why the optical structures should be aligned with the radio axis [Eales (1992) gives a possible explanation].

Notwithstanding this temptation, one selection effect makes it impossible to be sure that any difference is caused by cosmic evolution. Almost all the results above were obtained from observations of the bright 3C sample of radio sources (Laing, Riley and Longair 1983). Since 3C is a flux-limited sample, radio luminosity and redshift are tightly correlated (Fig. 1), which means that that any difference in the properties of low- and high-redshift radio galaxies could equally well be due to the difference in their radio luminosities as to the difference in their redshifts. There are also often explanations of the observed differences based on luminosity that are equally as plausible as those based on cosmic evolution. For example, the difference in emission-line luminosities seems to be most naturally explained by the idea that the emission-line gas is being photoionized by continuum emission from

the active nucleus; both the emission-line luminosity and the radio luminosity then scale with the energy output of the active nucleus (Rawlings & Saunders 1991), with the high emission-line luminosities of the HZRG's being caused by their high radio luminosities rather than by their redshifts.

This is especially true in the case of the alignment effect, because although it is possible to think of explanations based on cosmic evolution or even simply on the effect of the redshift (if the alignment effect is primarily a UV phenomenom, it will be more obvious to optical observations as the redshift increases), most of the suggested explanations are based on the high radio luminosities of the high-redshift 3C galaxies not on their redshifts. For example, the intensity and direction (E-vector perpendicular to the radio axis) of the polarized optical emission from a typical HZRG suggests a model in which the HZRG contains a quasar that we cannot see directly but which is emitting optical radiation along the radio axis in the plane of the sky, with the aligned optical component being light from the quasar that is scattered towards us (Tadhunter, Fosbury & di Serego Alighieri 1988). In this model the brightness of this extended emission, and thus the quality of the alignment between the radio and optical axes, will depend on the brightness of the quasar, and thus on the energy output of the central engine. Since the radio luminosity will also depend on this, this hypothesis makes the prediction that the strength of the alignment effect depends on the radio luminosities of the galaxies not on their redshifts. A similar prediction comes from the hypothesis that the alignments are caused by star formation being triggered along the axis of a radio source by the bowshock of the expanding source (McCarthy et al. 1987). Dunlop & Peacock (1993) have found evidence that the alignment effect is indeed related to radio luminosity rather than to redshift. They find that the K-band structures of 3C radio galaxies at $z \simeq 1$ are closely aligned with the radio axes, but that the K-band structures of sources from a faint radio sample whose K-band magnitudes suggest they are at a similar redshift to the 3C galaxies are not aligned with the radio axes.

As the last result illustrates, the way to disentangle the effects of redshift and radio luminosity is to compare the properties of a faint radio sample with those of a bright radio sample such as 3C. Although radio luminosity and redshift will be tightly correlated within the faint sample, when the two samples are considered together there will be a much larger range of radio luminosity at constant redshift than is available within a single flux-limited sample (the range of luminosity is given roughly by the ratio of the flux limits of the two samples), and similarly there will be a larger range of redshift at constant radio luminosity. Although redshifts have been measured for large numbers of HZRG's in faint radio samples (there are over 100 radio galaxies known at $z > 2$, for example—McCarthy 1993), most have been found using radio criteria designed to preferentially select high-redshift sources, and thus they form a biased sample. To give one example, McCarthy et al. (1991) observed a large number of sources selected from the Molongo Radio Catalogue with spectral indices greater than 0.9. The advantage of using this spectral-index criterion is that it is effective (for reasons that are not understood) at selecting the most luminous sources, and thus the ones that are at the highest redshifts. These also are the ones for which it is easiest to measure redshifts (line luminosity is correlated with radio luminosity [§5.1], and the high redshifts put bright lines in accessible parts of the spectrum). The disadvantage is

that introducing this criterion biases the sample in ways that are not properly undestood. The practical difficulty in the way of measuring redshifts for *all* the sources in faint radio samples has been the exhorbitant amount of telescope time needed, a problem that appears particularly daunting when one considers it took 30 years of observational work to do the same for 3C.

Over the last decade we and collaborators have been gradually obtaining optical, infrared and radio images, and, most importantly, redshifts for the sources in the faint samples of Allington-Smith (1982) and Eales (1985a), samples drawn respectively from the 408-MHz B2 survey and from the 151-MHz 6C survey, and both with flux limits about six times fainter than that of 3C. Radio samples selected at different frequencies contain different proportions of sources from the different radio morphological types (e.g. Peacock and Wall 1981), but since 3C was also carried out at a low frequency (178 MHz), comparisons of the faint samples with 3C should not suffer from this problem. Table 1 shows the parameters of the original samples. The two faint samples contain many sources in common, since they were selected in almost the same area of sky and have similar flux limits. The total number of sources in the original samples was 84. Three of the sources are now known to the result of the confusion of two or more sources within the telescope's beam, with the fluxes of the separate sources not falling within the flux limits of the samples, and the flux originally given for one source is now known to be wrong, which leaves 80 sources remaining within the samples.

We have now completed our observational study of these samples and have redshifts and infrared magnitudes for a large fraction of the sources, as well as many new radio maps and a limited amount of optical imaging data. The crucial data are the redshifts. Here we have redshifts for 72 (90%) of the 80 sources. Of the sources without redshifts, one is too close to a star for us to obtain either an image or a redshift, two sources are fairly bright galaxies (R $\sim$ 20), for which we believe we can reliably estimate redshifts (see below), one is a BL Lac object, and four appear too faint for us to be able to measure redshifts with 4m-class telescopes, despite several attempts. As far as we are aware, these samples are the first faint samples with such complete redshift information. Apart from three low-redshift galaxies, two quasars, and the source close to the star, we have infrared photometry, measured either with a single-element detector or with a camera, for all of the sources in the samples. The way we intend to present the data is as follows. The new radio maps have already been published (Naundorf et al. 1991; Law-Green et al. 1995a). This paper will present the infrared images and a subsequent paper (Rawlings et al. 1996—Paper II) will contain the optical spectra. A final paper (Paper III) will deal with some of the technical issues concerning the samples (some of the radio flux scales have changed since the original papers, for example) and will provide a compilation of all the data and a reference list.

At the same time, and often in the same papers, we will compare the data for the faint samples with that for 3C, in an attempt to determine whether the differences between the low-redshift and high-redshift 3C sources are genuinely caused by cosmic evolution. We have already used the faint samples to show that the physical sizes of double radio sources are smaller at high redshift as the result of cosmic evolution rather than being the result of a luminosity effect (Neeser et al. 1995). In this paper we turn our attention to Lilly

and Longair's (1984) discovery that high-redshift 3C galaxies are systematically brighter in the K-band than expected from the absolute magnitudes of radio galaxies at low redshift. Although this result is nicely in accord with one's preconceptions about galaxy evolution—stellar evolution should make galaxies brighter in the past!—in this paper we show that it is the high radio luminosities of the high-redshift 3C galaxies that are responsible for their bright K-band magnitudes. We will also consider the question of whether the strength of the alignment effect depends on radio luminosity. Paper II will address the question of whether the emission-line luminosity of a radio galaxy depends on its redshift or its radio luminosity and also the fundamental question of whether the comoving space density of radio galaxies reaches a maximum at some redshift.

The layout of this paper is as follows. We present the data in §2. We compare the Hubble diagrams of the faint samples and of the bright 3C sample in §3, and compare the alignment effect in the different samples in §4. We discuss the consequences of these comparisons in §5. We assume a Hubble constant of 50 km s^{-1} Mpc^{-1}.

2. Observations and Data Reduction

2.1. The Observations

Most of the observations were made during three observing runs. In 1994 Jan 16-18, we used the IRCAM infrared camera on the United Kingdom Infrared Telescope (UKIRT) to observe some of the sources in the infrared K-band (2.2 μm). IRCAM consists of a 58 $\times$ 62 element SBRC infrared array and has a plate scale of 0.62 arcsec $pixel^{-1}$. In 1995 Jan 18-20 we used the REDEYE camera on the Canada-France-Hawaii Telescope (CFHT) to observe sources in the K′-band. REDEYE consists of four 128 $\times$ 128 element HgCdTe mosaics butted together (there is a small gap between the two lower and two upper arrays) with a plate scale of 0.5 arcsec $pixel^{-1}$. The K′-band is similar to the K-band but is shifted to a slightly shorter wavelength in order to reduce the noise caused by the rapidly increasing thermal background in the long-wavelength part of the K-band filter. On 1995 Jan 25 we used the new IRCAM3 camera on the UKIRT to make observations in the K-band. IRCAM3 consists of a 256 $\times$ 256 element SBRC infrared array and has a plate scale of 0.286 arcsec $pixel^{-1}$. A handful of galaxies were observed with IRCAM or IRCAM3 during other regular observing runs or during service runs. We observed many of the galaxies in our sample with two or more of these cameras, which gives us a useful check on the photometric accuracy of our observations (§2.4). Table 2 lists the sources we observed and the instruments we used.

In all cases we used the standard technique of observing each galaxy at nine positions on a 3 $\times$3 grid with a spacing between gridpoints of 8 arcsec. As long as the background emission is either mainly produced by the sky, or is from the telescope but is spatially flat (Bunker 1996), this is a useful procedure, because an accurate flat field can be produced from the data themselves (§2.2). We typically integrated for about three minutes per position, and in many cases we repeated the sequence of nine observations several times. Total exposure times are given in Table 2. We photometrically calibrated our data by observations of standards from the list of Elias (1982), mainly 7th-magnitude stars, and from the UKIRT list of faint standards (10-14th magnitude), which appears on the UKIRT

pages of the worldwide web. Note that the REDEYE observations were made through a K′-filter but were calibrated using K-band standards. This means that to obtain proper K-band magnitudes from these observations we had to make a colour-correction. This is described in §2.2.

Since the size of IRCAM was not large enough in many cases for us to obtain astrometric information from objects visible on the final image, for most of the galaxies we used the following astrometric procedure. For each galaxy we first obtained an image of a nearby star with known position, then moved the telescope to the position of the radio galaxy and started observing. The position of the star on its image allowed us to determine where the radio galaxy should fall on its image with an accuracy of about 1 arcsecond.

2.2. Data Reduction

Since the galaxies we observed were very faint, the procedure we used to reduce the data, which used a combination of IRAF routines and our own programs, was quite elaborate and we give it here in some detail. It is very similar to the procedure used by Dunlop & Peacock (1993), but there are some differences. The first step was to correct for known bad pixels by replacing the value associated with each bad pixel by the median of the values in the surrounding pixels. The second step was to subtract from each image of the galaxy an image taken with the same integration time but with the shutter closed, the effect of this being to remove the dark current associated with the array. The next step was to construct a flat field, by first normalizing the images of each galaxy so that they had the same median value, and then making an image with the intensity at each pixel equal to the median of the intensities at the same pixel in the normalized images. After normalizing the flat field so that it had a mean value of unity, we divided each of the galaxy images by it.

At this point the usual step is to positionally align the images and then sum them, but we found that a couple of additional processing steps at this point significantly improved our images. First, there is the occasional pixel that clearly has a too high or too low value compared with the surrounding pixels but which does not appear in the list of known bad pixels. We searched for these pixels by looking for ones that differed by more than a threshold amount from the median of the surrounding pixels, the threshold being chosen by trial and error to result in the selection of the obviously bad pixels. We replaced each bad pixel by the median of the surrounding pixels. Second, on the IRCAM images, even after the flat-fielding step there were often large-scale gradients left on the images. We removed these using the IRAF program IMSURFIT which fits a polynomial surface to an image and then subtracts it from the image. The obvious danger in this is that if the order of the polynomial surface is too high, some flux will be removed from the objects on the image. In most cases we avoided this problem completely by only fitting the polynomial to areas of the array away from the object, and in practice we found that even when the object was not masked the step had no systematic effect on the magnitudes but did result in an improvement to the appearance of the final image. After these two additional steps we returned to the usual data-reduction sequence and positionally aligned the images and summed them. In the case of the REDEYE and the IRCAM3 data, we astrometrically aligned the images by measuring the position of a bright object visible in all the images.

In the case of the IRCAM images, with their smaller field of view, there was often no suitable object: in such cases we aligned the images by assuming that the positioning of the telescope had been accurate.

Figure 2 shows the final infrared images. We have plotted the positions of the radio components on the infrared images and identified the radio galaxy using two different techniques. For sources from which optical or infrared emission had not previously been detected we identified the radio galaxy, measured its position, and plotted the positions of the radio components on the infrared image using the astrometric procedure described at the end of §2.1. There is rarely any uncertainty as to which object is the radio galaxy, because there is usually either an object close to the radio core or, where there is no radio core, a single object midway between the radio lobes. The few cases where there is some ambiguity are discussed in detail in §2.3. The positions of these galaxies are given in Table 3, and our estimate of the accuracy of these position measurements is about an arc second. For sources where the radio galaxy had already been detected on an optical CCD image, we identified the radio galaxy on the infrared image by comparing the infrared image with the CCD image. In these cases it is the optical position that appears in Table 3, because the optical positions are usually more accurate than the positions we obtained from our IRCAM astrometry.

We measured magnitudes for all the galaxies using the IRAF program PHOT and circular apertures with a diameter of 5 arcsec and 8 arcsec. In some cases there were two objects close together, and in these cases we measured magnitudes for both objects. We measured the sky level by using the IRAF program FITSKY to estimate the mode of the intensity values in an annulus centered on the object, with the inner radius of the annulus being made sufficiently large that the annulus did not include any emission from the radio galaxy itself. We set the parameters of the FITSKY program so that it automatically excluded pixels which were clearly part of an object, and our use of the mode as the sky estimator was another precaution against our sky estimates being biased by the presence of objects in the annulus. The magnitudes are listed in Table 4. In cases where there is evidence that gradients in the sky background are making the large-aperture magnitudes unreliable we have listed only the small-aperture magnitudes.

The REDEYE observations were made through a K' filter, but calibrated by observing K-band standard stars (§2.1). Since the K' filter is shifted slightly in wavelength from the K filter, and since HZRG's have different colours from standard stars, there will be a systematic error in the resultant K magnitudes of the radio galaxies. We estimated the size of this error, using the transmission functions for the two filters, an average $H-K$ colour for the radio galaxies of 1 (Lilly & Longair 1984), and an average $H-K$ colour for the standard stars of 0, as 0.13 mag, in the sense that our initial estimates of the K magnitudes had to be made brighter by this value. Table 4 contains the corrected values.

We have made no correction for galactic extinction, since the high galactic latitudes of the B2/6C sources mean that the corrections will be both very small and uncertain. If we use the reddening map of Burstein and Heiles (1982), we find that two objects have corrections of about 0.01 mags to their K-magnitudes, with the corrections for the remaining objects having upper limits of about this value.

2.3. Notes on the Sources

0820+36: The three crosses in Fig. 2 show the positions of the hotspots and the radio core. There are two objects close to the radio core, and magnitudes are given for both in Table 4. The north-eastern object is close to the core, and we conclude that this is the true identification.

0822+34B: The three crosses in Fig. 2 show the positions of the hotspots and the radio core. There are two objects close to the radio core, and magnitudes are given for both in Table 4. The south-eastern object is closer to the core, and we have assumed that this is the radio galaxy.

0825+34: There are two objects close to the position of this small (7 arcsec) double source. There is no central component to help out with the astrometry, and either of the two objects might be the radio galaxy. Since the line joining the two objects is roughly aligned with the radio axis, it is possible that both objects are components of one object and that this system is an example of the alignment effect (§1). Since the chance of an unrelated galaxy coinciding with the radio source is less for a bright galaxy than a faint galaxy, we have assumed that the brighter of the two objects is the site of the active nucleus.

0901+35: There are two objects close to the position of this small (3 arcsec) double. The northern object is significantly closer to the position, and we have taken this to be the radio galaxy.

0905+39: We have discussed this source in detail in a separate paper (Law-Green et al. 1995b).

0918+36: We did not follow our standard astrometric procedure for this source. There are two objects visible on the infrared image and both are also visible on the R-band CCD image of Eales (1985b). Eales originally concluded that these objects were not associated with the radio source because radio galaxies almost always fall within 0.2θ of the point midway between the radio hotspots (Laing, Riley & Longair 1983), where θ is the angular distance between the hotspots, and neither of these objects was within that distance. However, the new radio map is much better than the original one, and the positions of the hotspots are slightly different, putting both the galaxies just within the 0.2θ circle. There is no radio core, but the brighter galaxy falls on a direct line between the hotspots and has the strong emission lines characteristic of a powerful radio galaxy, so it seems likely that this is the site of the active nucleus. The position in Table 3 is a previously unpublished measurement from the CCD image.

0943+39: The radio galaxy is unusually far from the point midway between the hotspots.

1016+36: The radio source is a 15-arcsec double and Allington-Smith suggests two possible identifications that are visible on his deep CCD image (Allington-Smith et al. 1982 and private communication). One is at (1950.0) 10 16 58.45, 36 37 49.7, and one at 10 16 58.59, 36 37 42.4. There is very little emission present on the infrared image between the radio hotspots, with the brightest object visible, the one marked, having K = 20.30. Although it is only a 3σ detection, it is probably real because the position we measure (10 16 58.48, 36 37 50.6) is very close to the position of one of Allington-Smith's objects. Although the ratio of the distances of the hotspots to this object is unusually far from one, we tentatively

conclude that it is the radio galaxy, but it is also possible that we have not yet detected the true identification.

1042+39: We did not follow our standard astrometric procedure for this source. However, when the UKIRT is pointed at an object (in this case the point midway between the radio hotspots), the object usually appears within a few arcsec of the centre of the image. Since there is only one object close to the centre of the infrared image, we are confident that this is the true identification. We cannot, however, give an accurate position for the galaxy.

1045+35A: There appears to be a cluster of galaxies surrounding the radio galaxy.

1100+35: The object between the radio hotspots is definitely the radio galaxy, since it coincides with the radio core. The object to the west, close to the western hotspot, is probably unrelated, since its spectrum looks quite different, resembling that of a low-redshift elliptical (Allington-Smith, private communication). The large difference between the K-magnitude measured by Lilly, Longair & Allington-Smith (1985) through a 12-arcsec aperture and the magnitude given here is probably explained if Lilly et al.'s larger aperture was centred slightly to the west of the radio galaxy and included the western object.

1143+37: We did not follow our standard astrometric procedure for this source. However, the pointing of the UKIRT is usually good to a few arcsec, and there is only a single object close to the centre of the image. It is only a 2.6σ detection, but the magnitude is consistent with that given by Lilly (1989).

1204+37: We have assumed that the object closest to the midpoint of this large (52 arcsec) double is the true identification. Evidence supporting this is that we succeeded in measuring a redshift by centering our slit on the radio midpoint (Rawlings et al. 1996).

1257+36: There are two features on the radio map of Law-Green et al. (1995a) that may be the radio core. Both are close to our proposed identification.

2.4. Photometric Checks

One check we have on our method is that we reduced all the IRCAM data twice, once using the method described in §2.2. and once while still on Mauna Kea using the standard STARLINK reduction package. Although the general schemes were similar, the specific programs were different and there were a number of minor methodological differences: for instance, in the latter case we estimated the sky level by measuring the mean level in small apertures that we placed in empty regions of the image. There was no systematic trend for one set of magnitudes to be brighter or fainter than the other.

A second way to investigate the photometric accuracy is to compare the magnitudes measured with the four different instruments: the three arrays—IRCAM, IRCAM3, and REDEYE—and the single-element photometer used by Lilly and collaborators. The photometry from the images generally agreed well with the photometry obtained by Lilly and collaborators using a single-element photometer (except in the case of $1100 + 35$, where the discrepancy is probably explained by a nearby object falling in Lilly's aperture—§2.3), agreeing with the conclusion of Dunlop and Peacock (1993) from a similar comparison for 3C galaxies. There are four objects where the magnitudes measured with the HgCdTe

camera (REDEYE) are significantly different from those measured with the InSb cameras (IRCAM/IRCAM3): $0905+39$, $1011+36$, $1017+37$, $1256+36$. Since the sizes of the differences are bigger for the larger aperture, the likely cause is residual gradients in the sky background, and indeed on careful inspection of the images it is often possible to see these gradients. Residual background gradients appeared to be particular problems for the IRCAM and REDEYE images, whereas the IRCAM3 images usually appeared much smoother. The median discrepancy between the small-aperture IRCAM/IRCAM3 magnitudes and the small-aperture REDEYE magnitudes is 0.09 mags, in the sense that the REDEYE magnitudes are brighter. However, given the small number of objects (nine) and the uncertainty in the correction from the K' magnitudes to K magnitudes, we do not believe there a serious photometric disagreement between the magnitudes measured with the HgCdTe REDEYE array and those measured with the InSb arrays.

3. The Hubble Diagram

In this section we compare the infrared Hubble diagrams (K versus z) of 3C and of the faint samples.

To construct the 3C Hubble diagram we use two samples of data. Lilly & Longair (1984) used a single-element photometer to obtain K-band photometry of 90 sources from the 3C sample of Laing, Riley & Longair (1983) which (a) were accessible from the UKIRT, (b) had not been classified by Laing et al. as either a quasar or a probable quasar, and (c) did not have redshifts < 0.03. There are an additional seven sources in the sample of Laing et al. satisfying these criteria which were not observed, four because they are close to bright stars, making reliable photometry difficult, and three because the deep optical images necessary for the success of Lilly and Longair's observational technique were not available (in one case because of the presence of a bright star, in the other two because the sources were late additions to the 3C sample). We are confident that the omission of these seven sources should not have biased Lilly and Longair's results and should not bias ours. In two cases the optical identification assumed by Lilly & Longair is incorrect (3C13 and 3C326—Le Fèvre et al. 1988; Rawlings et al. 1990), with the result that the K magnitude of the wrong galaxy was measured. We have discarded the data for these galaxies. The other sample is that of Dunlop & Peacock (1993), who obtained K-band images of 19 radio galaxies in the redshift range $0.8 < z < 1.3$ from the larger 3C sample listed by Spinrad et al. (1985). There are other 3C galaxies in this redshift range, but Dunlop and Peacock claim that the sample of galaxies they did observe is a representative sample of the galaxies in this redshift range. We are only interested in objects for which there is not already evidence that the optical/infrared light is mostly nonstellar, and so we have excluded from our analysis all radiogalaxies that Spinrad et al. (1985) classify as N-galaxies and ones that have the broad permitted emission-lines typical of quasars.

Many of the radio galaxies fall in both samples, and there is then the question of which magnitude to use. Dunlop & Peacock (1993) have shown that their magnitudes agree well with Lilly & Longair's magnitudes. We decided to use an array magnitude when one exists, simply because one is then sure about the position of the aperture and that it does not include the flux from some unrelated object. The redshifts for the 3C galaxies are mostly from Laing et al. or from Spinrad et al. (1985), with the exception of a few unpublished

redshifts mostly communicated to us by Spinrad (from whom an up-to-date list of 3C redshifts can be obtained).

For the faint sample there are several sources of infrared magnitudes: (a) the magnitudes listed in this paper, (b) IRCAM magnitudes given in Eales et al. (1993a, 1993b) and in Eales & Rawlings (1996), (c) magnitudes measured with the UKIRT single-element photometer by Lilly, Longair & Allington-Smith (1985) and by Lilly (1989). With the exception of the REDEYE magnitudes given in this paper, all the magnitudes have been measured with either the same instruments (or a very closely-related one, IRCAM3) used to measure the magnitudes of the 3C galaxies. The data reduction procedures have also been either the same or very similar. As for the 3C galaxies, if an array magnitude exists we used it. If more than one array magnitude exists, we used an IRCAM3 magnitude, because of the flatness of the IRCAM3 images, when possible, and when not the average of the REDEYE and IRCAM magnitudes, it being unclear which of these is preferable. For the galaxies for which there is a large difference between the IRCAM and the REDEYE magnitudes, we used the average of the magnitudes measured through the smaller aperture, for which the magnitude difference is always less (§2.4). Note that the photometric agreement between the different datasets (§2.4) is sufficiently good, that our choice of magnitudes should have a negligible effect on our results. The redshifts for the 6C/B2 galaxies that have not yet been published will be listed in Paper II. As we are only interested in objects for which there is not already evidence that the optical/infrared light is mostly nonstellar, we have again excluded from our analysis all the objects with the broad permitted emission-lines typical of quasars.

Now let us consider how to estimate magnitudes that correspond to the same metric aperture at all redshifts. Ideally, one choses a metric aperture, and then observes each galaxy through the aperture that gives this physical size at the redshift of the galaxy. In practice, this is not entirely possible, although one can approach this ideal by a careful choice of the metric aperture. The universe helps out to some extent, because above a redshift of 0.5 the physical distance subtended by a given angle depends only weakly on redshift. Since most of our photometry was obtained through an aperture of diameter eight arcsec or close to it, we have chosen 63.9 kpc as our metric diameter, since for $\Omega_0 = 1$ this corresponds to $\simeq 8''$ at a redshift of one. Thus much of our photometry was obtained through an aperture very similar to our chosen metric aperture. For most galaxies, though, some correction, however small, has still to be made to the measured magnitudes to convert them into magnitudes measured through the metric aperture. The standard way to do this is to assume that all radio galaxies have the same intensity profile, and then use this standard profile to correct the magnitudes. This is a very good approximation at low redshift, where most radio galaxies are giant ellipticals, and the intensity profile or "curve of growth" tabulated by Sandage (1972) is the one that has traditionally been used (e.g. Laing, Riley & Longair 1983). This is clearly the wrong thing to do here, because the structures of HZRG's often look very unlike those of low-redshift giant ellipticals (Fig. 2 and Dunlop & Peacock 1993). We decided to adopt the following compromise, which, on the one hand, avoids assuming that the structures of radio galaxies do not evolve and, on the other hand, avoids the necessity of estimating curves of growth for each individual galaxy. We divided the galaxies into those below a redshift of 0.6 and those above this

redshift, because this is the redshift above which the alignment effect is seen (McCarthy 1993). Below this redshift it seems a reasonable approximation that radio galaxies do have growth curves like that of a giant elliptical, and we used Sandage's growth curve to correct our magnitudes to the standard metric aperture. Above this redshift we assumed that the emission within an aperture of radius r is $\propto r^{\alpha}$ and derived a value for α of 0.35 from the median difference between the small-aperture and large-aperture magnitudes in Table 4 (0.18 mags). We then used this intensity profile to correct all the magnitudes of galaxies at $z > 0.6$ to the standard metric aperture. It is important to note that the aperture corrections are generally small. At $z > 0.6$ 75% of the galaxies have aperture corrections less than 0.05 mags.

Figure 3 shows the Hubble diagram for the two samples. There are some obvious visual differences between two distributions. We have adopted the following method for analysing those differences. There are two obvious redshifts at which to split the diagram. First, there are no 3C galaxies at $z > 1.8$ and so we have removed all the 6C/B2 galaxies above this redshift from our analysis. Second, the alignment effect starts to be seen at redshifts > 0.6 (McCarthy 1993), so this seems a natural redshift to split the data. In the two redshift bins—$0 < z < 0.6$ and $0.6 < z < 1.8$— we have used the following method of seeing whether the distributions are similar for the two samples. In each bin we fitted a straight line to the data points for 3C by minimizing the sum of the squared residuals in magnitude between the points and the line. We then plotted histograms of the residuals between the data points and the line for both the 3C and the 6C/B2 sample. The fitted lines are shown in Figure 4, the histograms in Figure 5.

Figures 5(a) and 5(b) show the residuals for the low-redshift bin. There is no obvious differences between the histogram for 3C and that for the faint sample, and this is borne out by a Mann-Whitney U-test, which shows that the null hypothesis that the two samples are drawn from the same underlying distribution is statistically acceptable. This agrees with the results of a study by Hill and Lilly (1991) of a sample of radio galaxies at $z \sim 0.5$. They showed that for this sample the absolute optical magnitude is independent of radio luminosity over a range of $\simeq$1000 in radio luminosity. Thus our result and that of Hill and Lilly agree with the conventional wisdom that low-redshift radio galaxies are 'standard candles' with a small range of absolute magnitude, and that the absolute magnitude is independent of radio luminosity.

Figures 5(c) and 5(d) show the residuals for the high-redshift sample. Here the distributions are clearly different, and application of the Mann-Whitney U-test shows that the probability that the null hypothesis, that the distributions are drawn from the same underlying distribution, is correct is $\simeq$0.01%. This is also very clear from Fig. 4. Almost all the B2/6C galaxies are fainter than the line that is the best fit to the 3C data. The median difference between the 3C and 6C/B2 residuals is 0.59 mags (a factor of 1.7 in intensity)‡. Since the only other difference between the 3C and B2/6C galaxies is one of radio luminosity (roughly a factor of 6), in this redshift bin there is a correlation between radio and infrared luminosity†.

‡ This is slightly less than the difference claimed in Eales & Rawlings (1996), the change being due to remeasurements of some of the redshifts.

† Because of the redshift, the emission we are detecting in the infrared K-band is being

We cannot think of any obvious way our analysis could have spuriouly generated this result. Although there are some differences between the magnitudes measured with different cameras (§2.4), the differences are much smaller than the size of the average difference between the magnitudes of the 6C/B2 and 3C galaxies. It would be possible to produce this result if we had systematically misclassified more 3C quasars as galaxies than 6C/B2 quasars as galaxies. If anything, though, we have probably erred in the opposite direction, since we excluded 3C sources classified in the literature as N-galaxies, whereas no such classifications exist for the 6C/B2 galaxies. Finally we consider the eight 6C/B2 galaxies that are not plotted in the Hubble diagram because they do not yet have redshifts. One of these we can ignore because the lack of a redshift is simply due to the presence of a nearby star, and thus its omission from the diagram does not bias the diagram in any way; two are relatively bright galaxies ($R \sim 20$), and have estimated redshifts which put them in the low-redshift bin; one is a BL Lac object; the remaining four might be galaxies in the high-redshift bin, and so, in principle, their omission might affect our result. The K-magnitudes of these four are 19.8, 19.0, 17.36, and 19.46. Three of these are among the faintest K-magnitudes that we have measured, and if these objects do fall in the high-redshift bin the true difference between the B2/6C and 3C galaxies will actually be greater. Therefore, it seems likely that the difference between the K-magnitudes of the B2/6C and 3C galaxies is a fundamental one.

It is possible to explain all the properties of the Hubble diagram—the result that there is no difference between the samples at low redshift, that there is a difference at high redshift, and Lilly and Longair's discovery that the infrared luminosities of 3C galaxies increase with redshift—by the following simple model. We will assume that there are two components to the near-infrared emission from a radio galaxy: starlight and nonstellar light. We will not worry about the nature of the second component until later (§5.1); for now we will assume that its strength is proportional to the power output of the active nucleus. Since the radio luminosity will also monotonically increase with the power output of the active nucleus (Rawlings & Saunders 1991), the nonstellar infrared component will be proportional to the radio luminosity. We will additionally assume that the starlight component does not depend on radio luminosity. There is no guaruntee that this model is correct, of course, but it is the least radical departure from our existing ideas about radio galaxies that we could think of; it keeps the idea that the galaxies themselves have a small range of absolute magnitude at a given redshift while incorporating the idea (for which there is evidence even at low redshift—Yee & Oke 1978) that there is a nonstellar component to the light from radio galaxies. If we assume this model, the properties of the Hubble diagram follow quite naturally. It explains why at low redshift there is no difference between the B2/6C and 3C galaxies: the radio luminosities of both sets of galaxies are then so low that the nonstellar infrared emission is swamped by the starlight from the galaxy. It explains why the 3C galaxies at $1 < z < 2$ have higher infrared luminosities than the B2/6C galaxies in the same redshift range: the 3C galaxies have higher radio luminosities and thus more nonstellar emission. Finally it explains why 3C galaxies at $z \sim 1$ are more luminous than those at $z \sim 0$: because of the correlation between radio

emitted by the galaxies at $\sim 1\mu$m, which is actually on the border between the infrared and optical wavebands.

luminosity and redshift in any flux-limited sample, 3C galaxies at high redshift have higher radio luminosities, and thus higher infrared luminosities, than those at low redshift. In contrast, Lilly & Longair's model cannot explain all the properties of the Hubble diagram. If stellar evolution is responsible for the increase in infrared luminosity of the 3C galaxies between now and $z \sim 1$, it should have a similar effect on the 6C/B2 galaxies, since the optical properties of the low-redshift 6C/B2 galaxies are indistinguishable from those of the low-redshift 3C galaxies.

4. The Alignment Effect in the Infrared

Since there is no agreement about the explanation of the alignment effect, any information about how it depends on redshift, radio luminosity, and on wavelength of observation is important. Rigler et al. (1992), in a study of 3C galaxies at $z \sim 1$, found that, in contrast to the optical structures, there is no evidence that the infrared structures are aligned with the radio structures. They also found that the infrared structures are generally less elongated than the optical structures. In contrast, Dunlop & Peacock (1993; henceforth DP), in a study of a very similar sample of 3C galaxies, found that the infrared structures of 3C galaxies at $z \sim 1$ are actually more closely aligned with the radio structures than the optical structures are, although they agreed with the conclusion of Rigler et al. that the infrared structures are generally less elongated. They extended their study of the alignment effect to galaxies with lower radio luminosities by selecting galaxies from a faint radio sample drawn from the Parkes radio catalogue with a similar range of K magnitude to their sample of 3C galaxies. As long as the relation between K magnitude and redshift is the same for both samples, the Parkes galaxies will lie in the same redshift range as the 3C galaxies, but will have lower radio luminosities. DP found that although the infrared structures of the 3C galaxies are closely aligned with the radio structures, the infrared structures of the Parkes galaxies are not, implying that the alignment effect is a function of radio luminosity.

We argued in the last section that the basic assumption of DP is not true: the relation between K magnitude and redshift is not the same for a bright and a faint radio sample, the relation for the faint sample being offset to fainter magnitudes. The effect of this will be that galaxies in DP's faint radio sample will actually lie at redshifts that are lower than the ones predicted from the 3C relation. Thus their two samples of HZRG's—the 3C sample and the Parkes sample—will not cover identical redshift ranges; the Parkes galaxies will generally be at lower redshift. We do not claim their result is invalid, because the main difference between the two samples, and thus the likely explanation of the difference in the alignment effect, is still likely to be one of radio luminosity rather than redshift, but this effect does produce some uncertainty in their result. However, we can reexamine the question, and hopefully dispel some of the uncertainty, because we can use redshifts rather than K magnitudes to compile a suitable sample of faint radio galaxies to compare with DP's 3C sample.

DP considered the redshift range $0.8 < z < 1.5$, and there are 15 B2/6C galaxies in this redshift range. Of these 15, there are nine which have both the FR2 radio structure (Fanaroff & Riley 1974) and for which there are infrared images. Because estimates by eye of the position angle of an infrared structure are uncertain, depending on such things as

the greyscale used to display the image, DP developed an objective method of estimating the position angle. They calculated the intensity moments ($< Ixy >$, $< Ix^2 >$, $< Iy^2 >$) of each galaxy, using only pixels within an angle θ of the centre of the galaxy, and then they diagonalized the matrix of moments to find the position angle. To maximize the signal-to-noise of their estimates, they only considered pixels whose intensities were greater than $0.3I_{max}$, I_{max} being the maximum intensity of each galaxy. Their choice of θ was governed by the size of the radio source. For sources with angular sizes greater than 8 arcsec they used a value for θ of 4 arcsec; for sources with a diameter of less than 5 arcsec they a value for θ of 2.5 arcsec; and for sources with a diameter between 5 and 8 arcsec they used a value for θ equal to half the diameter of the source (see DP for a justification of this). We used exactly the same technique as DP. For galaxies where we had more than one image, if possible we estimated the position angle from a REDEYE image, because these had the best angular resolution (FWHM usually less than one arcsec), and if a REDEYE image was not available we preferred the IRCAM3 image to the IRCAM image.

Our estimates of the position angle are given in Table 5, and a histogram of the differences between the infrared and radio position angle is shown in Figure 6. We used a Kolmogorov-Smirnov one-sample test (Siegel 1956) to examine whether the data are consistent with a uniform distribution (i.e. no alignment effect). The result was tantalising, since we found that the chance that this null hypothesis is correct is <20%; the limit arising because the standard statistical tables (Siegel 1956) consider the probability that the null hypothesis is true against all possible alternatives, whereas we are only interested in the alternative hypothesis that the data is bunched up towards 0°—and the data is in this direction. Nevertheless, in contrast to the histogram for 3C (DP), there is no evidence of a very strong effect, supporting DP's conclusion that the alignment effect is a phenomenom associated mostly with the most luminous sources.

5. Discussion

5.1. The Nature of the K-band Excess

In §3 we sketched a possible explanation of the various features of the Hubble diagram by suggesting there are two components to the near-infrared emission from a radio galaxy: light from stars and a nonstellar component that is produced by the active nucleus and whose strength is correlated with the total radio luminosity. We claimed that this is the least radical change one can make to our existing ideas about radio galaxies and still explain the Hubble diagram. However, at that point we did not fill in any of the details of the sketch. There are three ways one can do this.

One possibility is that some of the K-band emission is actually due to emission lines rather than to continuum processes. It has been known for a while that emission-line luminosity is correlated with either radio luminosity or redshift (Rawlings et al. 1989), and a comparison of emission-line fluxes for the B2/6C galaxies with those for 3C shows that the true correlation is with radio luminosity (Rawlings et al. 1996). So if the K-band flux is being produced by emission lines in the K-band filter, one would expect a correlation between K-band luminosity and radio luminosity. However, at these redshifts the potentially troublesome lines are [SIII] 953.2 and He I 1083.0, which have lower equivalent widths than

[OIII] 500.7 and Hα, which significantly "pollute" the K-band magnitudes of HZRG's at z $>$ 2 (Eales & Rawlings 1993, 1996; Eales et al. 1993b). The infrared spectroscopy that we have done of 3C galaxies at z $\sim$ 1 (Rawlings, Lacy & Eales 1991, and unpublished data) shows that the contribution of emission lines is *at most* 25% of the total K-band emission. Therefore it seems unlikely that the infrared-radio correlation is caused by line emission.

An alternative is to propose that there are quasars in the centres of the radio galaxies, that the optical/infrared continuum emission from these quasars is proportional to the radio luminosity, and that these quasars are behind screens of dust which are just thick enough to conceal them from our view at optical wavelengths but not at infrared wavelengths. If this model is correct, a large fraction of the near-infrared light from a high-redshift 3C galaxy is actually coming directly from a quasar. There must be enough dust present for the broad permitted lines and bright continuum emission that are characteristic of a quasar to be hidden at optical wavelengths, because otherwise the object would already have been classified as a quasar. There are a number of things in favour of this model. First, it is broadly in line with the popular "unified models" (e.g. Barthel 1989). Second, Serjeant et al. (1996) have shown that for quasars with steep radio spectra—that is quasars with similar radio properties to most 3C radio galaxies—radio and optical luminosity are correlated. This does not of course prove that the model is right, merely that if there are quasars in the centres of the radio galaxies obscured by a small screen of dust then there is reason to expect the near-infrared continuum emission to scale with the radio luminosity. Finally, we have shown that for one object this model does seem to be correct. The radio source 3C 22, which has a redshift of 0.937, is classified as a radio galaxy, because it has narrow permitted optical emission lines. However, we have recently observed this with an infrared spectrometer and found that Hα, which is redshifted into the near-infrared J-band, is broad (Rawlings et al. 1995). The lack of broad permitted lines in the optical spectrum and the red spectral energy distribution can be explained if we are viewing a quasar through a screen of dust with a visual extinction of $\sim$ 2 mags.

Nevertheless, although there is some evidence in favour of this model, it is not entirely satisfactory. First, it does not explain why there is a near-infrared alignment effect for high-redshift 3C galaxies but not for high-redshift B2/6C/Parkes galaxies (§4). If anything one would expect the reverse. If the light from a high-redshift 3C galaxy is dominated by light directly from the central quasar, then this light would make the alignment effect, which must be connected to the other component of the light, harder to see. Second, there are reasons to think 3C 22 might be different from the other high-redshift 3C galaxies. It has a one-sided radio jet (Fernini et al. 1993), it has by far the brightest K-magnitude of any of the high-redshift 3C galaxies, and of the objects observed by DP it is the one whose K-band image looks most like that of a quasar; none of the infrared structures of the other 3C and Parkes galaxies is so clearly dominated by a single unresolved source.

It is possible to avoid these problems and retain the general outline of the model if, instead of the quasar light being seen directly, it is scattered towards us by either dust or electrons. There is evidence that this process operates at optical wavelengths. The degree of polarization of the optical light from high-redshift 3C galaxies is typically around 10% and the electric vector of the polarized light is usually perpendicular to the radio axis (e.g. Tadhunter et al. 1992; di Serego Alighieri, Cimatti & Fosbury 1993), exactly what is

expected if the central quasar in a radio galaxy is completely hidden from our direct view but is illuminating dust or electrons along the radio axis (in the unified scheme of Barthel [1989] assumed to be close to the plane of the sky), which scatter the quasar light towards us. This scheme would both explain the features of the Hubble diagram and explain why the alignment effect is seen clearly for the 3C galaxies but not for the 6C/B2/Parkes galaxies. An obvious argument against this scheme is that the spectral energy distributions of HZRG's increase to longer wavelengths, whereas the scattering efficiency of electrons remains constant, and that of dust decreases, towards longer wavelengths. However, it is relatively easy to think of a model that could produce more light being scattered in the infrared than at optical wavelengths if one allows for the absorption produced by dust. If there is a fairly large amount of dust along the radio axis, the scattering particles, whatever they are, may see little optical emission, and although the scattering efficiency may be less at longer wavelengths there may be much more light to scatter. There is some limited evidence that in the optical waveband, the degree of polarization decreases to longer wavelengths (Cimatti et al. 1993), but the evidence is not compelling and, even if correct, it would be still be possible for the degree of polarization to start increasing again. The real way to test this model is to perform imaging polarimetry in the near infrared, and we are in the process of doing this.

We argued that this overall model is the least radical departure from our existing ideas, but this does not mean that it is correct. It is quite possible that the true explanation is completely different. We will just mention one idea as an example of more exotic explanations. Even at a redshift of one, galaxies with radio luminosities as high as those of 3C galaxies are quite rare, with there being $\sim 10^2$ such objects over the whole sky. Our current ideas about the physics of double radio sources suggests there are two ways to increase the low-frequency radio luminosity of a galaxy (see Rawlings & Saunders 1991; Eales 1992). One is to increase the energy flowing along the jet, roughly the power of the central engine, and one is to increase of the density of the gas surrounding the radio lobes. Suppose that to generate the radio luminosity of these rare ultraluminous 3C galaxies both factors are necessary: the most powerful central engines and also the densest gas. We know very little about galaxies at a redshift of one, but it seems quite likely that the most extensive and densest distributions of gas are likely to be associated with the most massive stellar systems. Thus, if this idea is correct, the 3C galaxies at $z \sim 1$ are the most massive systems around at this epoch and the K-band light is still starlight. Of course this is only a sketch (a similar and more detailed sketch is given in Eales, 1992), but it seems to us that this is as likely to be true as the less exotic sketch shown above.

5.2. Galaxy Evolution

Figure 7a shows the Hubble diagram and the predictions of various models. The broken lines show the predictions of various evolutionary models. We have produced these using the models of Bruzual & Charlot (1993), which are contained in the "Galaxy Isochrone Synthesis Spectral Evolution Library" (GISSEL). These models allow the user to investigate the ultraviolet/optical/infrared properties of a galaxy for any history of star formation and for a number of different initial mass functions. The specific GISSEL model we have used is the one for an instantaneous burst of star formation with a Salpeter IMF

with a lower mass cutoff of 0.1 $M_\odot$ and an upper mass cutoff of 125 $M_\odot$. The three models correspond to three different assumptions about the history of star formation in a radio galaxy, although in each case the star formation is assumed to occur at $z >> 1$. The continuous line is the prediction of a no-evolution model†. We have normalized all the models so that their predictions pass through the low-redshift points. As Lilly & Longair (1984) discovered, the 3C galaxies at $z \sim 1$ are significantly brighter than the no-evolution curve, and agree rather well with the predictions of the evolution models.

However, we have concluded that the bright K-magnitudes of 3C galaxies at $z \sim 1$ are connected to the high radio luminosities of these objects, not to their redshifts, and so the agreement between the magnitudes and the evolutionary models is actually fortuitous. Is it still possible to draw any conclusions about galaxy evolution from this diagram? It turns out that it *is* possible to draw some conclusions, although only tentative ones, and ones which depend on the assumption one makes about the explanation of the relationship between infrared and radio luminosity.

First, let us assume that our conservative hypothesis is correct, that there are two components of the near-infrared light: light from stars and a nonstellar component that is produced by the active nucleus and whose strength is correlated with the total radio luminosity. At any redshift, the nonstellar component will be less important for the 6C/B2 galaxies than for the 3C galaxies, and so inferences about galaxy evolution drawn from the 6C/B2 K-z relation are more likely to be correct than those drawn from the 3C relation. In Figure 7a, the B2/6C galaxies actually follow the no-evolution curve out to a redshift close to two. This is rather a surprise, because stellar evolution should be making the galaxies brighter in the past. However, it is a phenomenom that is also seen in the K-z relation for galaxies found in deep surveys. Although the K-z relation for normal galaxies does not have the small dispersion seen for radio galaxies, and so it is not useful to try and fit a curve to the points, it is useful to look at the upper envelope of the distribution—the line that traces the brightest K-magnitude seen for normal galaxies at any redshift. Songaila et al. (1995) have found that, out to $z \sim 1$, this line also does not show the brightening expected from stellar evolution. Both for our radio galaxies and the normal galaxies,

† All that is necessary to calculate this is the average spectral energy distribution of low-redshift radio galaxies. A minor problem is that although there are published spectral energy distributions of adequate spectral resolution in the optical waveband (e.g. Coleman, Wu & Weedman 1980), the only spectral information in the near infrared is broad-band colours. We have overcome this by using the GISSEL models to find a star-formation history for a radio galaxy that produces, at the current epoch, both the observed near-infrared colours and the observed optical spectral energy distribution. The models can then be used to generate a zero-redshift spectral energy distribution in the near infrared of sufficient spectral resolution to generate a K-z curve. All that we are really doing is finding a physically plausible way of interpolating between the near infrared magnitudes of a low-redshift radio galaxy, and although in principle this does not produce a unique solution, with a variety of star-formation histories capable of generating the same observed optical and near-infrared properties at low redshift, in practice we found that different star-formation histories, as long as they could reproduce the observed low-redshift properties, lead to virtually identical K-z curves.

there are two obvious possible solutions to this paradox. First, we may have assumed the wrong cosmology. For a low-density Friedmann universe (Fig. 7b), the 6C/B2 galaxies are brighter than the no-evolution model at z $\sim$ 1. Second, there may be another type of evolution occurring that is operating in the opposite direction to that of stellar evolution. All models of galaxy formation based on hierarchical clustering (Press & Schechter 1974; White et al. 1983) make the firm prediction that the structures of galaxies should evolve at the same time as the stars in them evolve. Indeed, simulations based on these models produce images that look remarkably like the linear lumpy images of HZRG's (e.g. Fig. 3, Baron & White 1987). Since this process will make the luminosities of galaxies increase with time, it would tend to cancel out the efffect of stellar evolution, and thus might explain the overall lack of evolution seen in the Hubble diagram.

These two possible conclusions depend, of course, on whether the basic hypothesis is correct. They also depend on one other assumption. We have implicitly assumed that although the near-infrared light from 3C galaxies at z $\sim$ 1 is dominated by nonstellar light, the near-infrared light from the high-redshift 6C/B2 galaxies is mostly from stars, whereas it is possible that this is still "polluted" by nonstellar light. If that is so, the magnitudes of the *stellar* components of the 6C/B2 galaxies would be displaced upwards in the Hubble diagram from the existing points, strengthening the evidence for merging if $\Omega_0 = 1$, and possibly requiring it for $\Omega_0 = 0$ as well. This, however, does not seem too likely because optical spectroscopy of 3C galaxies has found evidence of a significant stellar component even in these objects (Lacy & Rawlings 1994; Lacy et al. 1995; Stockton, Kellog & Ridgeway 1995). The obvious way to test this idea is to look at the Hubble relation of an even fainter radio sample, where the luminosity of the nonstellar component should be even less. We and other groups are in the process of doing this. As yet, there is a single intriguing result. Dunlop et al. (1996) have obtained a deep spectrum with the Keck Telescope of a radio galaxy at a redshift of 1.55. The spectrum is very similar to the rest-frame UV spectrum of a low-mass main-sequence star, implying that it is dominated by stars, and the galaxy's radio luminosity is many times less than that of 6C/B2 galaxies at the same redshift. Nevertheless, it is in a similar place in the Hubble diagram to the B2/6C galaxies (Figs 7), suggesting that the light from the B2/6C galaxies is dominated by stars as well, and that, after discarding the polluted 3C galaxies, the old assumption that radio galaxies are "standard candles" is valid out to a z $\sim 1-2$.

As we noted in the previous section, merely because an assumption is the most conservative one does not necessarily make it correct; and if we start out with a different explanation of the relation between radio and infrared luminosity we end up with a different conclusion about galaxy evolution. As an example of more exotic explanations, let us consider again the suggestion in §5.1 that, at z $\sim$ 1, the most radio-luminous sources (those in 3C) can only exist in the most massive galaxies, whereas slightly less radio-luminous sources (6C/B2) can survive in less massive galaxies. At the current epoch radio galaxies with a wide range of radio luminosity are always associated with the most massive galaxies, so this hypothesis leads to an opposite conclusion to the hypothesis above. It is no longer correct to compare high-redshift 6C/B2 galaxies with low-redshift radio galaxies, because one is then comparing apples and oranges, or rather the most massive galaxies at the current epoch with galaxies further down the galaxy luminosity function at z $\sim$ 1. Instead,

it is reasonable to compare the 3C galaxies at z $\sim$ 1 with low-redshift radio galaxies, because one is then comparing the most massive galaxies at both epochs. One then of course reaches precisely the same conclusion as Lilly & Longair (1984): the most massive galaxies are brighter at z $\sim$ 1 than they are today, possibly because of stellar evolution. We have now discussed the consequences for galaxy evolution of two possible explanations of the relation between radio and infrared luminosity, but there are undoubtedly other possible explanations. Thus, to summarize, one can draw conclusions about galaxy evolution, but they depend on the assumptions one makes about the explanation of the relation between radio and infrared luminosity.

The discussion above applies only to redshifts less than $\sim$ 2, because, as Fig. 7 shows, above this redshift the galaxies are systematically brighter than the no-evolution model and the dispersion in the K-z relation also appears to increase. We have already suggested this second result in a previous paper (Eales et al. 1993a), in which we looked at the K-magnitudes of the handful of radio galaxies that were then known to have redshifts greater than two and which had K-magnitudes. This sample did not form a statistically-complete sample and for this reason our conclusion was very tentative. Here we can be much more confident, because we are comparing flux-limited samples of sources for almost all of which we have redshifts and K-magnitudes. Let us consider the data in two natural redshift bins: the 3C and the 6C/B2 galaxies together at z $<$ 0.6, and the 6C/B2 galaxies at z $>$ 1.8, the maximum redshift in 3C. As in the earlier paper, we fit straight lines to the points in both samples, minimizing the sum of the root mean squared residuals in magnitude. The dispersion around the line for the low-redshift points is 0.47 mags; for the high-redshift bin it is 1.29 mags. This is a larger difference than we found in the previous paper, it is for a larger and more uniform sample of HZRG's, and the result is thus much more secure. Although we are missing redshifts for four faint galaxies, it is easy to see by inspection of the Hubble diagram that including these in the high-redshift bin would not significantly change this result.

Both of these changes in the K-z relation at z $\sim$ 2 are suggestive of galaxy formation. If the stars in a galaxy form at a constant rate in a specified period of time, the maximum optical luminosity of the galaxy occurs at the end of this period (Charlot & Bruzual 1991). The minima in the evolutionary curves shown in Figure 7a occur at this time, and several of the 6C/B2 galaxies have magnitudes very similar to the ones predicted for the end of this formation period. An increase in dispersion is also a predicted feature of the epoch of galaxy formation. This follows because the luminosity of a galaxy will change most rapidly immediately after the period in which most of the stars are formed (e.g. Figure 5 of Charlot & Bruzual 1991). Therefore, as long as radio galaxies do not form at exactly the same instant, the range of their luminosities should be greatest during the formation epoch. However, although both of these properties of the K-z relation do suggest that we are seeing the 6C/B2 galaxies at z $>$ 2 either shortly after or during the epoch in which most of the stars in the galaxies formed, there are two factors that have to be considered. First, at z $>$ 2 there are potentially bright emission lines that fall in the K-band and may inflate the K-band fluxes. Second, the 6C/B2 galaxies at z $>$ 2 have higher radio luminosities than those at lower redshift, and it is possible that the kind of selection effect we have argued is responsible for the bright magnitudes of the 3C galaxies at z $\sim$ 1 is also

responsible for the bright magnitudes of the 6C/B2 galaxies at $z > 2$. We have addressed all of these issues in a second paper (Eales & Rawlings 1996).

6. Summary

We have obtained redshifts and infrared images for a sample of faint B2/6C radio sources whose fluxes are about six times fainter than those of sources in the bright 3C sample. By comparing the infrared structures and Hubble relations of the bright and faint samples, we have reached three conclusions:

(1) At low redshift radio galaxies are "standard candles", with radio galaxies almost always being giant ellipticals with a small spread of absolute magnitude. However, at $z \sim 1$ we find that the 6C/B2 galaxies are on average $\simeq$0.6 mags fainter in the K-band than 3C galaxies at the same redshift. The 6C/B2 galaxies have radio luminosities which are about six times fainter than those of 3C galaxies at the same redshift, and thus at high redshift radio and infrared luminosity are correlated.

(2) The infrared stuctures of B2/6C galaxies at $z \sim 1$ are less clearly aligned with their radio structures than 3C galaxies at this redshift, supporting the conclusion of Dunlop & Peacock (1993) that the strength of the alignment effect depends on radio luminosity.

(3) Out to a redshift of ~ 2 the 6C/B2 galaxies follow a no-evolution model ($\Omega = 1$), but above this redshift the galaxies are systematically brighter than this model and the dispersion in the K-z relation is about 2.7 times that at low redshift.

The most conservative (in terms of changes to our present ideas) explanation of the first result is if there are two components to the near-infrared emission from a radio galaxy: light from stars and a nonstellar component that is produced by the active nucleus and whose strength is correlated with the total radio luminosity. If the nonstellar light is coming directly from the active nucleus (seen through a screen of dust to hide, at optical wavelengths, the signs of a quasar), the model cannot explain the second result; but if the nonstellar light is being seen indirectly, scattered towards us by either dust or electrons, the model can explain both the first and second result. If either of these ideas is correct, Lilly & Longair's conclusion that the the bright K-band magnitudes of 3C galaxies at $z \sim 1$ are due to stellar evolution is incorrect; they are actually due to the high radio luminosities of these objects.

In this scenario, since the infrared magnitudes of the 6C/B2 galaxies will be less "polluted" by nonstellar emission, it may still be possible to make inferences about galactic evolution by looking at the 6C/B2 K-z diagram. Out to $z \sim 2$, these galaxies follow the no-evolution curve, in contradiction to the prediction that stellar evolution should be making galaxies brighter in the past. Possible ways out of this paradox are if we live in a low-density universe or if merging is making galaxies fainter in the past. However, we emphasize that inferences about galactic evolution depend critically on the assumptions one makes about the cause of the correlation between infrared and radio luminosity, and it is possible to think of qualitative explanations which have the light from 3C galaxies still dominated by stars and which "save" Lilly and Longair's result.

The obvious explanation of the third result is if at $z > 2$ we are seeing radio galaxies that are in the process of formation, because both the brighter magnitudes and the large dispersion in the K-z relation are what is expected during the epoch of galaxy formation. We have discussed this result further in Eales & Rawlings (1996).

Acknowledgements

We thank James Dunlop for kindly obtaining several images for us, and the staff at the CFHT and the UKIRT for their support during our various observing runs, in particular Robin Arsenault, Colin Aspin, Tim Carroll, Dolores Walther, and Thor Wold. We thank the referee, Pat McCarthy, for his helpful comments. This research has been financially supported at various stages by the National Science and Engineering Research Council of Canada and by the Particle Physics and Astronomy Research Council (PPARC) of the UK. The United Kingdom Infrared Telescope is operated by the Royal Observatory Edinburgh on behalf of the PPARC.

Refernces

Allington-Smith, J.R. 1982, MNRAS, 199, 611.

Allington-Smith, J.R., Perryman, M.A.C., Longair, M.S., Gunn, J.E. & Westphal, J.A. 1982, MNRAS, 201, 331.

Baron, E. & White, S.D.M. 1987, ApJ, 322, 585.

Barthel, P.D. 1989, ApJ, 336, 606.

Bruzual, G. & Charlot, S. 1993, ApJ, 405, 538.

Bunker, A. 1996, Ph.D. thesis (Oxford), in preparation.

Burstein, D. & Heiles, C. 1982, AJ, 87, 1165.
Chambers, K. C., Miley, G. K. & van Breugel, W. 1987, Nature, 329, 604.

Charlot, S., & Bruzual, G.A. 1991, ApJ, 367, 126.

Cimatti, A., di Serego Alighieri, S., Fosbury, R.A.E., Salvati, M. & Taylor, D. 1993, MNRAS, 264, 421.

Coleman, G.D., Wu, C-C., & Weedman, D.W. 1980, ApJ suppl., 43, 393.

Di Serego Alighieri, S., Cimatti, A. & Fosbury, R.A.E. 1993, ApJ, 404, 584.

Dunlop, J. & Peacock, J. A. 1993, MNRAS, 263, 936.

Dunlop, J. & Peacock, J. A., Spinrad, H., Dey, A., Jimenez, R., Stern, D. & Windhorst, R. 1996, Nature, 381, 581.

Eales, S. A. 1985a, MNRAS, 217, 149.

Eales, S.A. 1985b, MNRAS, 217, 167.

Eales, S. A. 1985c, MNRAS, 217, 179.

Eales, S. A. 1992, ApJ, 397, 49.

Eales, S.A. & Rawlings, S. 1993, ApJ, 411, 67.

Eales, S.A. & Rawlings, S. 1996, ApJ, 460, 68.

Eales, S.A., Rawlings, S., Dickinson, M., Spinrad, H., Lacy, M., & Hill, G. 1993a, ApJ., 409, 578.

Eales, S.A., Rawlings, S., Puxley, P., Rocca-Volmerage, B., & Kuntz, K. 1993b, Nature, 363, 140.

Elias, J.H., Frogel, J.A., Matthews, K. & Neugebauer, G. 1982, AJ, 87, 1029.

Fanaroff, B.L. & Riley, J.M. 1974, MNRAS, 167, 31p.

Fernini, I., Burns, J.O., Bridle, A.H. & Perley, R.A. 1993, AJ, 105, 1690.

Hill, G.J. & Lilly, S. 1991, ApJ, 367, 1.

Jackson, N. & Rawlings, S. 1996, MNRAS, in press.

Laing, R.A., Riley, J.M. & Longair, M.S. 1983, MNRAS, 204, 151.

Lacy, M. & Rawlings, S. 1994, MNRAS, 270, 431p.

Lacy, M., Rawlings, S., Eales, S.A. & Dunlop, J.S. 1995, MNRAS, 273, 821p.

Law-Green, J.D.B., Alexander, P., Allington-Smith, J.R., van Breugel, W.J.M., Eales, S.A., Leahy, J.P., Rawlings, S.G. & Spinrad, H. 1995a, MNRAS, 274, 939.

Law-Green, J.D.B., Eales, S.A., Leahy, J.P., Rawlings, S. & Lacy, M. 1995b, MNRAS, 277, 995.

Le Fèvre, O., Hammer, F., Nottale, L., Mazure, A., & Christian, C. 1988, ApJ, 324, L1.

Longair, M. S., Best, P.N. & Rottgering, H.J.A. 1995, MNRAS, 275, 47p.

Lilly, S.J. 1989, ApJ, 340, 77.
Lilly, S. J. & Longair, M. S. 1984, MNRAS, 211, 833.

Lilly, S.J., Longair, M.S. & Allington-Smith, J.R. 1985, MNRAS, 215, 37.

McCarthy, P.J. 1991, AJ, 102, 518.

McCarthy, P.J. 1993, ARAA, 31, 639.

McCarthy, P. J., Spinrad, H., Djorgovski, S., Strauss, M. A., van Breugel, W. & Liebert, J. 1987, ApJ, 319, L39.

McCarthy, P.J., van Breugel, W. J. M. & Kapahi, V. K. 1991, ApJ, 371, 478.

McCarthy, P.J., van Breugel, W. J. M., Kapahi, V. K., & Subrahmanya, C.R. 1991, AJ, 102, 522.

Naundorf, C., Alexander, P., Riley, J.M. & Eales, S.A. 1992, MNRAS, 258, 647.

Neeser, M., Eales, S.A., Law-Green, J.D., Leahy, J.P. & Rawlings, S. 1995, ApJ, 451, 76.

Peacock, J.A. & Wall, J.V. 1981, MNRAS, 194, 331.

Press, W.H. & Schechter, P. 1974, ApJ, 187, 425.

Rawlings, S. et al. 1996, in preparation (Paper II).

Rawlings, S., Lacy, M. & Eales, S. 1991, MNRAS, 251, 17p.

Rawlings, S., Lacy, M., Sivia, D. & Eales, S., 1995, MNRAS, 274, 428.

Rawlings, S. & Saunders, R. D. E. 1991, Nature, 349, 138.

Rawlings, S., Saunders, R., Eales, S. & Mackay, C. 1989, MNRAS, 240, 701.

Rawlings, S., Saunders, R., Miller, P., Jones, M.E., & Eales, S.A. 1990, MNRAS, 246, 21p.

Rigler, M.A., Lilly, S.J., Stockton, A., Hammer, F., and Le Fèvre, O. 1992, ApJ, 385, 61.

Sandage, A. 1972, ApJ, 173, 485.

Serjeant, S. et al. 1996, MNRAS, submitted.

Siegel, S. 1956, *Nonparametric statistics for the behavioural scientists*, (McGraw-Hill).
Songaila, A., Cowie, L.L., Hu, E.M. & Gardner, J.P. 1994, ApJ suppl., 434, 114.

Spinrad, H., Djorgovski, S., Marr, J., & Aguilar, L. 1985, PASP, 97, 932.

Stockton, A., Kellogg, M. & Ridgway, S.E. 1995, ApJ, 443, L69.

Tadhunter, C.N., Fosbury, R.A.E. & di Serego Alighieri, S. 1988, *BL Lac objects: proceedings of the Como conference 1988*, eds Maraschi, L., Maccacaro, T. & Ulrich, M.-H. (Springer Verlag), p79.

Tadhunter, C.N., Scarrott, S.M., Draper, P. & Rolph, C. 1992, MNRAS, 256, 53p.

White, S.D.M., Huchra, J., Latham, D. & Davis, M. 1983, MNRAS, 203, 701.

Yee, H.K.C. & Oke, J.B. 1978, ApJ, 226, 753.

Figure Captions

Figure 1: Radio luminosity at 151 MHz versus redshift for the 3C sample of Laing, Riley & Longair (1983; open circles) and for the 6C sample (filled circles). The tight correlation between radio luminosity and redshift seen for both samples arises because the samples include only sources which fall above or between certain flux limits.

Figure 2: Infrared images of sources in the 6C and B2 samples. North is always up, east to the left. The white crosses on the images mark the positions of radio components (for astrometric details see the text). Where the image is an IRCAM or IRCAM3 image the whole field is shown, a rectangle 52×55 arcsec^2 in size in the case of the IRCAM images and one 89×89 arcsec^2 in size in the case of the IRCAM3 images. Because of the mosaicing technique, the full sensitivity is only achieved over the central 20×23 arcsec^2 for the IRCAM images and over the central 57×57 arcsec^2 for the IRCAM3 images. Where the image is a REDEYE image, only the central 89×89 arcsec^2 of the image is shown, the full sensitivity being achieved over the whole area. The instrument used to produce each images is as follows: $0820+36$ (IRCAM), $0822+34$B (IRCAM), $0822+39$ (REDEYE), $0825+34$ (IRCAM), $0848+34$ (IRCAM), $0901+35$ (IRCAM), $0905+39$ (REDEYE), $0918+36$ (IRCAM), $0943+39$ (IRCAM3), $1011+36$ (REDEYE), $1016+36$ (IRCAM), $1017+37$ (REDEYE), $1042+39$ (IRCAM), $1045+34$ (REDEYE), $1045+35$A (IRCAM), $1045+35$B (IRCAM), $1100+35$ (IRCAM3), $1123+34$ (REDEYE), $1129+37$ (IRCAM3), $1141+35$ (IRCAM), $1143+37$ (IRCAM), $1204+35$ (IRCAM3), $1204+37$ (IRCAM), $1212+38$ (IRCAM), $1217+36$ (IRCAM3), $1230+34$ (IRCAM), $1256+36$ (REDEYE), $1257+36$ (REDEYE), $1301+35$ (IRCAM).

Figure 3: Hubble diagram for the 3C sample (filled circles) and the 6C/B2 sample (open circles). For details of how the diagram has been constructed see the text.

Figure 4: The same Hubble diagram as in Fig. 3 but with the addition of the results of our simple statistical comparison of the 3C sample (filled circles) and the 6C/B2 sample (open circles). The vertical lines show the redshift above which the alignment effect starts to be seen ($z = 0.6$ - McCarthy 1993) and the maximum redshift of galaxies in 3C ($z = 1.781$). The dashed line shows our fit to the 3C points in the redshift range $0.6 < z < 1.782$, and the continuous line our fit to the 3C points at $z < 0.6$.

Figure 5: Histograms of the difference between the magnitude of a galaxy and the best-fitting line in Fig. 4. Figures 5(a) and 5(b) are for the 3C and 6C galaxies in the low-redshift ($z < 0.6$) bin, and Figures 5(c) and 5(d) are for the 3C and 6C galaxies in the high-redshift ($0.6 < z < 1.8$) bin.

Figure 6: Histogram of the absolute difference between K-band and radio position angle for B2/6C galaxies with the FR2 radio structure in the redshift range $0.8 < z < 1.5$.

Figure 7: Same as Fig. 3 except that the curves show the relations predicted, first, if radio galaxies do not evolve and, second, for various assumptions about their star-formation histories. The diagram in Fig. 7a is for $\Omega_0 = 1$ and that in Fig. 7b for $\Omega_0 = 0$.

The continuous lines in both diagrams are the curves expected if radio galaxies show no evolution (see footnote for details of how this is calculated). The other lines show the relations predicted if all the stars in a radio galaxy form at a continuous rate for a fixed period and if there is no star formation after this period. The lowest line is for a model in which the star formation starts at $z = 10$ and lasts 1 Gyr, the middle line for one in which the star formation starts at $z = 100$ and lasts 1 Gyr, and the highest line for one in which the star formation starts at $z = \infty$ and lasts 0.1 Gyr. The last model gives the least possible evolution between now and $z \sim 1$ for a single-burst model, since 0.1 Gyr is a typical galactic free-fall time and is thus the minimum period in which all the stars can form. Details of how these curves are calculated are given in the text. The triangle shows the position of the high-redshift galaxy with a low radio luminosity observed by Dunlop et al. (1996).

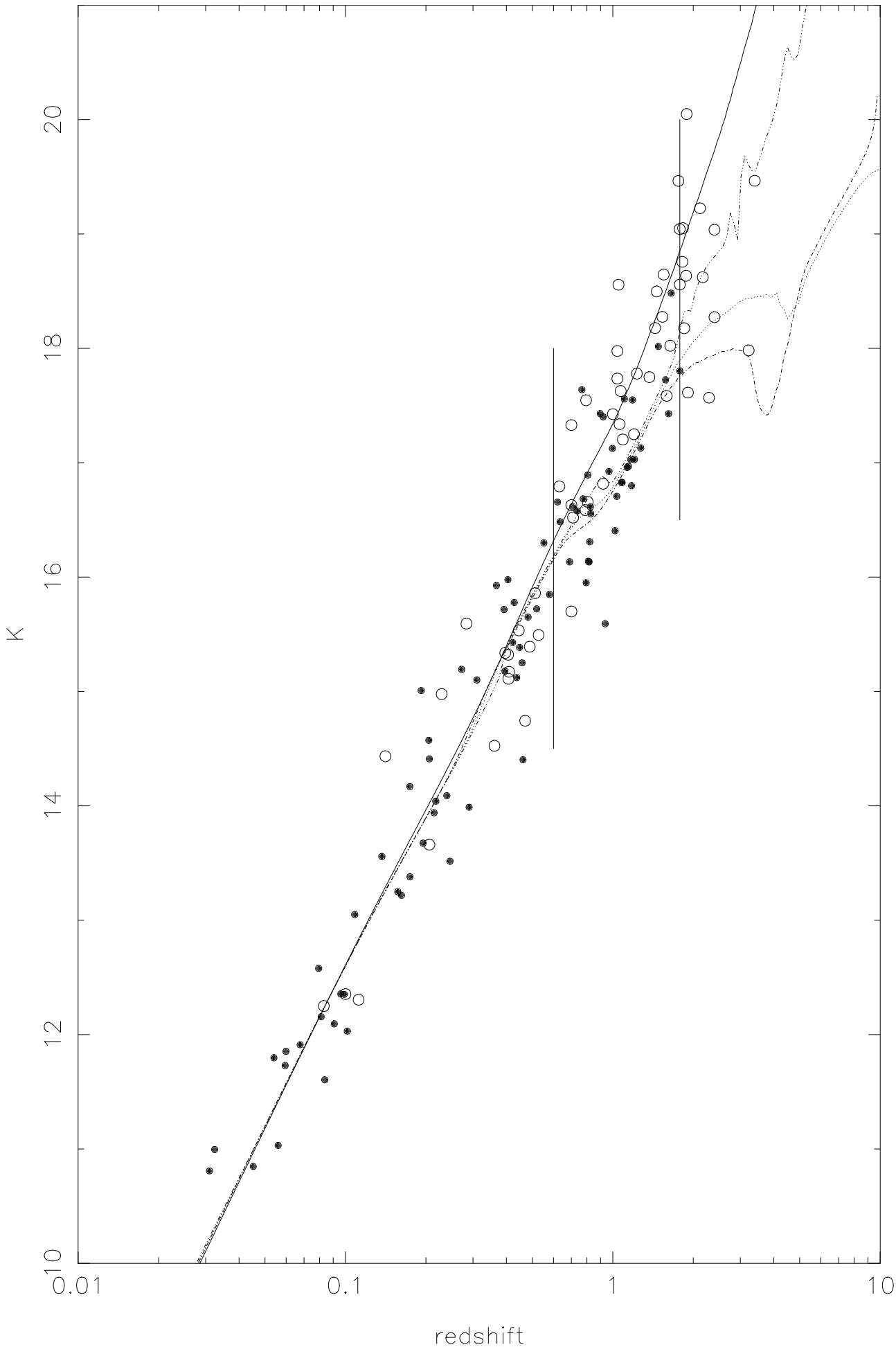
K
redshift
10
12
14
16
18
20
0.01
0.1
1
10

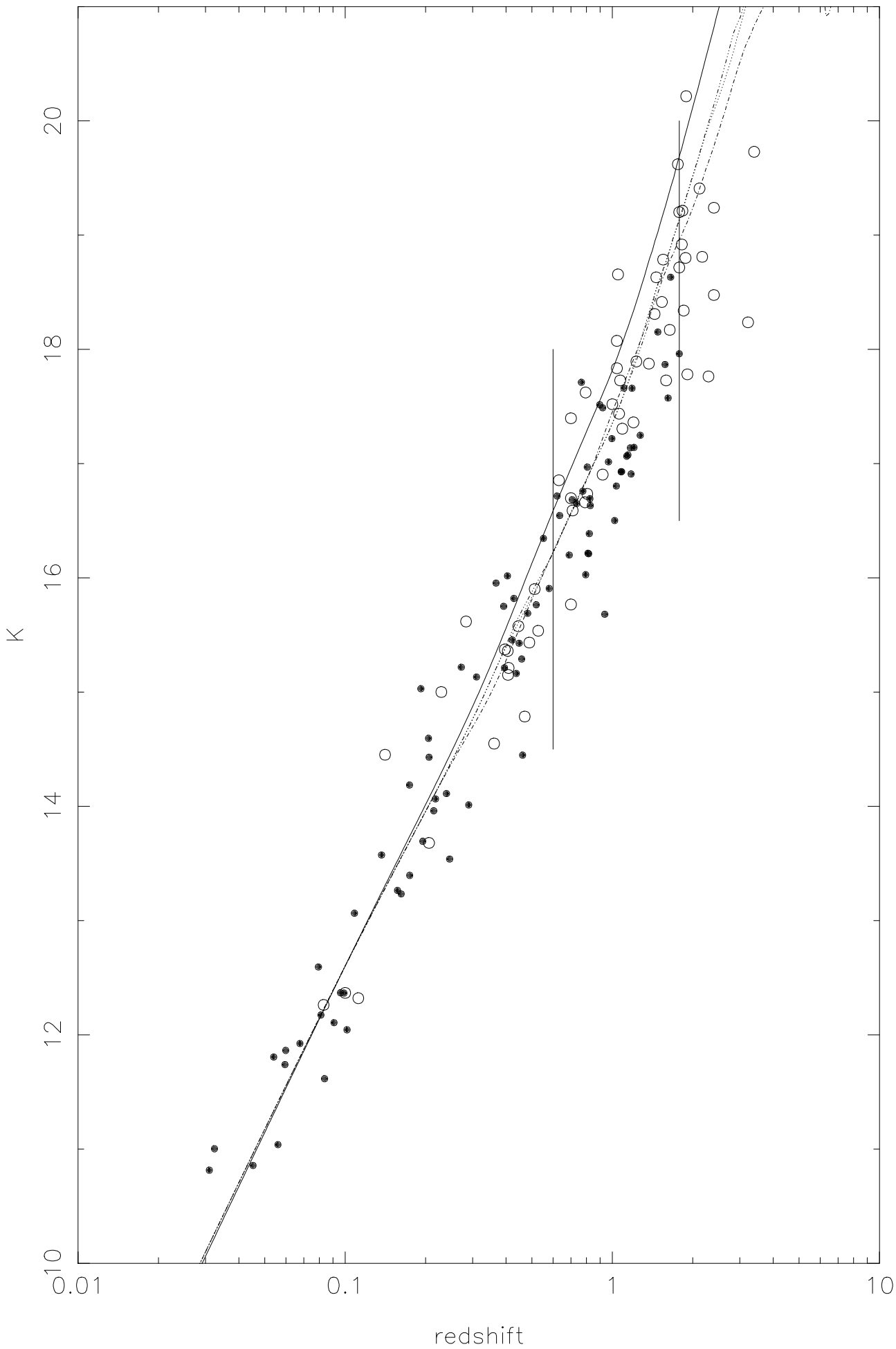
K
redshift
10
12
14
16
18
20
0.01
0.1
1
10